Available online at www.sciencedirect.com
SCIENCE DIRECT®
Coordination Chemistry Reviews 249 (2005) 3007–3024
COORDINATION CHEMISTRY REVIEWS
www.elsevier.com/locate/ccr

Review

Structural and spectroscopic models of the A-cluster of acetyl coenzyme a synthase/carbon monoxide dehydrogenase: Nature's Monsanto acetic acid catalyst

Todd C. Harrop, Pradip K. Mascharak *

Department of Chemistry and Biochemistry, Thimann Laboratories, University of California, Santa Cruz, CA 95064, USA

Received 10 January 2005; accepted 18 April 2005
Available online 1 June 2005

Contents

Abstract

Acetyl coenzyme A synthase/carbon monoxide dehydrogenase (ACS/CODH) is a bifunctional enzyme present in a number of anaerobic bacteria. The enzyme catalyzes two separate reactions namely, the reduction of atmospheric CO_2 to CO (CODH activity at the C-cluster) and the synthesis of acetyl coenzyme A (ACS activity at the A-cluster) from CO, CH_3 from a corrinoid iron-sulfur protein, and the thiol coenzyme A. The structure(s) of the A-cluster of ACS/CODH from *Moorella thermoacetica* revealed an unprecedented structure with three different metallic subunits linked to each other through bridging Cys-S residues comprising the active site. In these structure(s) a Fe_4S_4 cubane is bridged via Cys-S to a bimetallic metal cluster. This bimetallic cluster contains a four-coordinate Ni, Cu, or Zn as the proximal metal (to the Fe_4S_4 cluster; designated M_p), which in turn is bridged through two Cys-S residues to a terminal square planar Ni(II) (Ni_d, distal to Fe_4S_4) ligated by two deprotonated carboxamido nitrogens from the peptide backbone. It is now established that Ni is required at the M_p site for the ACS activity. Over the past several years modeling efforts by several groups have provided clues towards understanding the intrinsic properties of the unique site in ACS. To date most studies have focused on dinuclear compounds that model the M_p–Ni_d subsite. Synthesis of such models have revealed that the Ni_p sites (a) are readily removed when mixed with 1,10-phenanthroline (phen) and (b) can be reduced to the Ni(I) and/or Ni(0) oxidation state (deduced by EPR or electrochemical studies) and bind CO in terminal fashion with ν_{co} value similar to the enzyme. In contrast, the presence of Cu(I) centers at these M_p sites do not bind CO and are not removable with phen supporting a non-catalytic role for Cu(I) at the M_p site in the enzyme. The Ni_d site (coordinated by carboxamido-N/thiolato-S) in these models are very stable in the +2 oxidation state and not readily removed upon treatment with phen suggesting that the source of 'labile Ni' and the NiFeC

* Corresponding author. Tel.: +1 831 459 4251; fax: +1 831 459 2935.
E-mail address: pradip@chemistry.ucsc.edu (P.K. Mascharak).

doi:10.1016/j.ccr.2005.04.019

signal arises from the presence of Ni at the M_p site in ACS. This review includes the results and implications of the modeling studies reported so far.

Keywords: Acetyl coenzyme A synthase; A-cluster; Model complexes; CO binding

1. Introduction

Acetyl coenzyme A synthase/carbon monoxide dehydrogenase (ACS/CODH) is a bifunctional enzyme present in a number of acetogenic, methanogenic, and sulfate-reducing bacteria and is a key player in the Wood–Ljungdahl pathway of autotrophic carbon fixation to convert CO or CO_2 into cell carbon [1–3]. The enzyme catalyzes two very important biological processes namely, the reversible reduction of atmospheric CO_2 to CO (at C-cluster, Eq. (1)) and the synthesis of acetyl coenzyme A from CO, CH_3 from a corrinoid iron-sulfur protein (CH_3CoCFeSP), and the thiol coenzyme A (at A-cluster, Eq. (2)) (Scheme 1). Interest in this enzyme stems from the organometallic reactions it catalyzes, analogous to the Monsanto acetic acid process, as well as its use of the greenhouse gas CO_2 as substrate. The crystal structure of the A-cluster (responsible for ACS activity e.g. acetyl CoA assembly) of ACS/CODH from the bacteria *Moorella thermoacetica* (f. *Clostridium thermoaceticum*) has been solved only recently [4,5]. Two independent research groups have shown that the A-cluster consists of a trimetallic core designated as [Fe_4S_4–S–M_p–S_2–Ni_d] where M_p (proximal metal to Fe_4S_4 cubane) can be Ni(II), Zn(II), or Cu(I), S represents bridging Cys-S residues and Ni_d is the metal site distal to the cubane. That three different metal ions can occupy an enzyme's active site has prompted several research groups to study smaller metal clusters that mimic the A-cluster site in ACS/CODH and sparked quite an intriguing discussion as to which metal is responsible for catalysis. In this regard, properly designed synthetic model systems could provide key clues toward questions regarding the identity of the metal(s) that promotes catalytic activity and the overall mechanism of the high energy C–S thioester bond formation in acetyl CoA synthesis. It is also expected that selected models may serve as efficient catalysts for the acetylation of a variety of organic substrates. This review highlights the synthetic efforts to model the A-cluster site reported so far in hope of gaining an understanding of the purpose of the metal(s) present at the M_p site and their overall mechanistic relevance. The review will cover some modeling approaches before the ACS/CODH structure was solved (from 1991 to 2003), but will mainly focus on models synthesized after the structure was published (from 2003 to 2004). Also, a brief discussion on the structure and properties of the enzyme itself has been included as the background of the review.

2. Background

2.1. Properties and structures of the A-cluster of ACS/CODH

The A-cluster of ACS/CODH has been shown to exist in two known oxidation states namely, the fully oxidized (diamagnetic) A_{ox} state and the one electron reduced (paramagnetic) A_{red} state [1]. The source of the electron for A-cluster reduction is currently uncertain although some suggest that the electron originates from the Fe_4S_4 cluster or some other cluster site in the protein (B or D clusters). However, recent biochemical studies have ruled out electron transfer from the Fe_4S_4 cluster since the rate is too slow for reduction to occur during each catalytic cycle [6]. Under CO atmosphere, A_{ox} is readily reduced to the A_{red}-CO state that exhibits a characteristic EPR signal called the NiFeC signal with *g* values at 2.08, 2.07, and 2.03 [1,7,8]. The NiFeC designation comes from the observed hyperfine broadening of the EPR spectrum upon isotopic substitution with ^{61}Ni, ^{57}Fe, and ^{13}CO [7,8]. The A_{red}-CO state is also characterized by the appearance of a strong single carbonyl stretching band (ν_{co}) in the IR spectrum of the protein at 1996 cm^{-1}, consistent with a terminally bound M–CO unit [9–10]. One other interesting feature of the A-cluster is the loss of ∼30% of the Ni content of the enzyme (called 'labile Ni') upon treatment with the bidentate chelator 1,10-phenanthroline (phen) [11]. When ACS/CODH is titrated with phen, both the NiFeC signal and the synthase activity disappear. This suggests that 'labile Ni' is a requirement for ACS activity [12]. Reconstitution of phen-treated ACS with $NiCl_2$ replenishes both the activity and the NiFeC EPR signal [12]. Interestingly, CODH activity is not affected

C-cluster (CODH Activity):

$$CO_2 + 2e^- + 2H^+ \rightleftharpoons CO + H_2O \quad (1)$$

A-cluster (ACS Activity):

$$CO + CH_3\text{-Co(III)-CFeSP} + CoASH \rightleftharpoons CH_3{-}\overset{\overset{O}{\|}}{C}{-}SCoA + Co(I)\text{-CFeSP} + H^+ \quad (2)$$

Scheme 1.

by phen treatment. ACS/CODH also accepts a methyl group from methylated corrinoid iron-sulfur protein (CH_3CoFeSP) to form a M–CH_3 adduct [6,13,14]. No EPR signal is associated with this binding, a fact that suggests a diamagnetic or integer spin state during CH_3^+ binding to the A-cluster [13]. However, the order of substrate binding, CO versus CH_3^+, to the A-cluster during acetyl CoA assembly is still largely unknown. The oxidation state of the Fe_4S_4 cubane during catalysis is also unknown although many groups have proposed that it exists in the $[Fe_4S_4]^{2+}$ or $[Fe_4S_4]^+$ form [1]. The results of Mössbauer, EPR, and UV/Vis studies on this cluster are consistent with a diamagnetic $[Fe_4S_4]^{2+}$ cluster in the resting state of ACS/CODH [7,15,16]. Since the ACS activity is also inhibited by excess CO [17], it is evident that Nature regulates the amount of CO delivered to the A-cluster during acetyl CoA synthesis.

The crystal structure of the bifunctional ACS/CODH from the model acetogen *M. thermoacetica* has been solved independently by two research groups [4,5]. The first structure of ACS/CODH, solved by Drennan and coworkers to 2.2 Å resolution, revealed that the enzyme exists as a 310 kDa symmetric $\alpha_2\beta_2$ heterodimer, a shape similar to that observed with electron microscopy [1,4]. The β-domain forms the center portion of the protein and houses the B, C (CODH site), and D Fe_4S_4 clusters. This domain structurally resembles the β-domain of the monofunctional CODH enzymes from *Carboxydothermus hydrogenoformans* [18] and *Rhodospirillum rubrum* [19] to a high extent. At each end of the protein complex lies the α-subunit that contains the A-cluster site responsible for acetyl CoA assembly. A 67 Å long hydrophobic channel connects the C-cluster to the A-cluster. This channel is proposed to be responsible for CO diffusion to the A-cluster during acetyl CoA synthesis. Indeed this channel could be used to synchronize cluster activity such that during acetyl CoA synthesis, the conformational changes in the protein quaternary structure are optimized along the various steps of the catalytic pathway. The α-subunit consists of three separate domains with all ligands to the A-cluster originating from domain 3 [4]. A dominant feature of the α-subunit is the large cavity among the three domains. The interactions among the three domains are not extensive with a small buried-surface area (1600 $Å^2$). This allows facile rearrangements at the domain interface to provide large molecules like CoASH and CoFeSP access to the A-cluster.

The structures of the C- and A-cluster sites revealed for the first time, the architecture of the sites of CO_2 reduction and acetyl CoA assembly, respectively. The structure of the C-cluster resembles that of the C-cluster of the monofunctional CODH from *R. rubrum* with a Fe–[$NiFe_3S_4$] cluster [4,19]. However, the identity of the metals at the A-cluster is quite interesting and unprecedented in biology. This cluster consists of a bimetallic site coordinated to a Fe_4S_4 cubane (Fig. 1) [4]. The bimetallic site contains a distorted tetrahedral Cu(I) ion connected to the Fe_4S_4 cubane via bridging Cys509. Furthermore, the Cu(I) center is ligated to two more bridging Cys-S

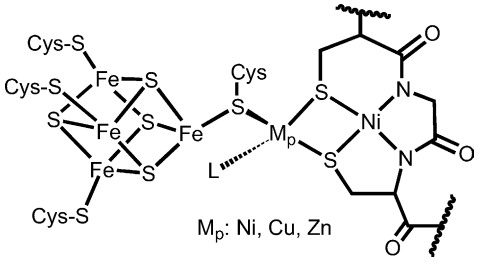

Fig. 1. Schematic drawing of the trimetallic site found in the A-cluster of ACS/CODH. M_p represents Ni(II), Cu(I), Zn(II) ions. L is an unidentified non-protein ligand.

residues (Cys595 and Cys597) that are bound to a square planar Ni(II) center. Two deprotonated carboxamido nitrogens from the peptide backbone (Gly596 and Cys597) are also bound to this Ni(II) center to afford a NiN_2S_2 coordination sphere (Fig. 1).

The second crystallographic study of ACS/CODH from the same bacterial source by Fontecilla-Camps and coworkers revealed several features that are somewhat different from the first structure [5]. Although the overall $\alpha_2\beta_2$ quaternary structure, organization of the protein subunits, structure of the C-cluster and the hydrophobic channel linking C- and A-cluster are the same as that noted in the Drennan structure [4], the structures of the α-subunits as well as the metal content at the A-cluster in each subunit are quite different. Indeed, the two α-subunits flanked at opposite ends in the overall protein structure exhibit two different conformations [5]. One α-subunit, α_c, is in a closed conformation. This resembles the α-subunit in the Drennan structure [4] and has limited access to solvent. The other α-subunit, α_o, is in an open conformation and has a larger exposed surface allowing greater solvent and substrate (CoASH) accessibility. The A-cluster in α_c-subunit, A_c, contains the same cuboidal Fe_4S_4 cluster as well as the distal NiN_2S_2 (Ni_d) unit but contains a distorted tetrahedral Zn(II) ion at the proximal (M_p) site (Fig. 1) [5]. In addition to the three bridging Cys-S donors, the coordination sphere around the Zn(II) center is completed by a tightly bound and unidentified heterodiatomic exogenous ligand. The A_c cluster is therefore similar to that in the Drennan structure [4] since Zn(II) and Cu(I) ions are isoelectronic and exhibit similar coordination geometries. However, the A-cluster in the α_o-subunit, A_o, contains a square planar Ni(II) center at the M_p site (along with the same Ni_d and cubane units, Fig. 1) [5]. The Ni(II) center here also contains an unknown exogenous ligand to complete its coordination sphere. One other noted difference between the two structures is that in the solvent exposed open conformation, A_o, the CO diffusion channel is closed and ∼20 Å away from the M_p site. Quite in contrast, in the closed conformation A_c, the CO channel is open with its ending directly on top of the M_p site. Thus, it appears that Nature has designed an appropriate maneuvering of subunits such that the potentially toxic CO gas molecule does not leak out of the protein or inhibit acetyl CoA synthesis when ACS/CODH is in the open con-

formation. Also, the capturing of two different coordination geometries at the M_p site suggests that the M_p site has a flexible and expandable coordination sphere during the acetyl CoA assembly process.

The presence of three different transition metals at one enzyme active site was never observed in any metalloenzyme before. Also, the presence of Cu(I) at the A-cluster site was quite a surprise since it had never been seen in other preparations of this enzyme. Although some reports correlate the Cu content at M_p with ACS activity [20], more recent evidence points toward Ni being the M_p metal that promotes synthase activity [21–25]. In addition, Svetlitchnyi et al. have determined the structure of ACS/CODH from another chemolithoautotroph *C. hydrogenoformans* that contains Ni at the M_p site [26]. It is now evident that Ni occupies the M_p site in the catalytically active enzyme and both Cu and Zn found in the crystals had their origin in the promiscuity of adventitious metal ion capture by the M_p site. The presence of deprotonated carboxamido nitrogens at the Ni_d site is also interesting. Indeed, coordination of peptide nitrogen in metalloenzymes is quite unusual with only the oxidized P-cluster of nitrogenase [27], nitrile hydratase (NHase) [28], and Ni-containing superoxide dismutase (Ni-SOD) [29] being other known examples. In fact, the basal plane N_2S_2 Cys-X-Cys motif (giving rise to N_2S_2 coordination) observed at the A-cluster Ni_d site bears remarkable resemblance with the Cys-X-Cys motif in NHase. These structural features of the A-cluster of ACS/CODH have raised a series of challenges to the bioinorganic chemists to solve such as what intrinsic properties do the coordinated ligands impart on each metal center and how does the whole metal cluster catalyze the overall assembly of acetyl CoA.

2.2. Mechanism(s) of acetyl coenzyme A synthesis by ACS/CODH

The mechanism of acetyl coenzyme A synthesis (ACS) is largely unresolved at this time. Several mechanisms with competing hypotheses (diamagnetic and paramagnetic) have been proposed before and after the most recent structure determinations. Before crystallographic characterization of the A-cluster site of ACS, many researchers believed that this site comprised a four-coordinate Ni(II) center coordinated by two Cys-S residues, one N donor, and another Cys-S that is bridged to an Fe_4S_4 cubane [1]. In the paramagnetic mechanism proposed by Ragsdale and coworkers, binding of CO to the Ni(I) center gives rise to a Ni(I)–CO unit responsible for the NiFeC signal [30,31]. A CH_3^+ moiety, donated by the methylated corrinoid iron-sulfur protein (CH_3CoCFeSP), then oxidatively adds to the Ni(I)–CO site generating an octahedral Ni(III) center with CH_3 and CO bound *cis* to each other. The Ni(III) oxidation state in this mechanism is short lived due to electron transfer from the cubane to generate an octahedral Ni(II) species. Next, CO insertion or methyl migration results in a pentacoordinate Ni(II)–$COCH_3$ species, a step that assists coordination of $CoAS^-$ and formation of acetyl CoA via attack of the acetyl group on the $CoAS^-$ moiety (both bound at the same Ni center). In the diamagnetic mechanism proposed by Lindahl and coworkers [13], the starting point is a pentacoordinate Ni(II) center with one extra N donor in the coordination sphere compared to the one in the Ragsdale mechanism [31]. Also, the oxidative addition of the CH_3^+ cation to the Ni(II) center does not proceed in the classical organometallic fashion. The oxidation state of the Ni center does not change and the two electrons responsible for the formation of the Ni–CH_3 bond come from nearby Cys-S donors (one electron each) affording a disulfide bond with one sulfur of the disulfide moiety still coordinated to Ni(II). Binding of CO to this Ni(II) site affords an octahedral intermediate with CH_3 and CO bound in *cis* position. Hereafter, the Lindahl mechanism is similar to that proposed by Ragsdale i.e. methyl migration/CO insertion then generates the Ni(II)–$COCH_3$ species that eventually binds $CoAS^-$ to afford acetyl CoA and the starting Ni(II) unit. Several aspects of these mechanisms are still controversial including the order of substrate binding (CO versus CH_3) as well as the oxidation state of the Fe_4S_4 cluster during catalysis.

Following the determination of the crystal structure(s) of the ACS A-cluster site, two "new" mechanisms have been proposed based on the metal center present at the M_p site. Fontecilla-Camps and coworkers propose that CO binds to Ni(0) at the M_p site to afford a tetrahedral $Ni(0)_p$ center in the closed conformation [5]. Oxidative addition of CH_3^+ to this $Ni(0)_p$–CO site then generates the open conformation and a square-pyramidal $Ni(II)_p$ center with CO and CH_3 bound in *cis* position. Next, CO insertion into the $Ni(II)_p$–CH_3 bond affords a $Ni(II)_p$–$COCH_3$ moiety. Finally, attack of $CoAS^-$ at the carbonyl carbon gives rise to acetyl CoA. This last step regenerates the $Ni(0)_p$ site and the coordination around Ni_p reverts back to trigonal pyramidal. As a consequence, the protein changes to the closed conformation (opening the CO tunnel) and the cycle starts back again [5]. Interestingly, the Fe_4S_4 and Ni_d sites do not participate in any redox events during the catalytic cycle in this mechanism. Their roles are restricted to metallation of the sulfurs of the $Ni_p(Cys\text{-}S)_3$ unit to facilitate redox chemistry at this site. Although the presence of a $Ni(0)_p$ site is still largely controversial, this mechanism does seem to account for many of the observed properties of the A-cluster [1,2]. For example, there is literature precedence for formation of Ni-bound acetyl group in small model Ni(0) complexes upon binding of CO and CH_3 groups (in *cis* configuration) [32–36]. Although the researchers discount the catalytic viability of the species exhibiting the NiFeC signal in this diamagnetic mechanism, it is quite plausible that a Ni(I) center can also be supported in this environment and would be positioned close enough to the Fe_4S_4 cluster to exhibit the expected EPR broadening upon isotopic substitution. The second "in silico" mechanism, proposed by Hall and coworkers, also begins with Ni(0) at the M_p site [22]. However, the addition of CO and CH_3^+ results in a square planar $Ni(II)_p$ center via de-ligation of one of its μ_2-cysteinyl-S_{Nid} bonds. Formation of the acetyl group then

affords a trigonal planar Ni(II)–acetyl species which binds $CoAS^-$. This adduct eventually rearranges to produce acetyl CoA and regenerates the $Ni(0)_p$ site. One must note at this point that participation of Ni(0) in a biological system has so far been unprecedented. The occurrence of $Ni(0)_p$ has not been established and there is no consensus for its existence in the A-cluster of ACS/CODH [37].

3. Model complexes and their reactivities

3.1. Required features and synthetic difficulties

The desire to understand the unique chemistry that occurs at the trimetallic core of the ACS/CODH A-cluster has prompted syntheses of models (analogues) of the active site utilizing designed ligands that mimic the coordination environment observed in the protein. This 'synthetic analogue approach', a paradigm in bioinorganic chemistry, has provided many insights into the intrinsic properties of metal centers in a variety of metalloenzymes so far [38]. The requirements of a good model of the ACS/CODH A-cluster are as follows:

(1) A terminal Ni(II) center (Ni_d model) that is coordinated by two carboxamido-N and two thiolato-S donors affording a diamagnetic d^8 Ni(II) center in a N_2S_2 square planar coordination geometry.
(2) A second metal center (M_p model), where M = Ni(II), Cu(I), or Zn(II), bridged to the $[NiN_2S_2]$ unit through both sulfur donors. In addition, a third metallosulfur donor arising from a Fe_4S_4 cubane, and a fourth labile ligand (L) are also present to give rise to a $M_p(S_3L)$ site in square planar or tetrahedral geometry.
(3) The Ni(II) center (M_p or Ni_d site mimic) is reducible to the Ni(I) oxidation state and is capable of binding CO to afford a Ni(I) EPR signal (NiFeC signal) with g values around 2.
(4) The model complex in the reduced form binds one CO in terminal fashion and one CH_3 group to the dimeric M_p–Ni_d portion and exhibit a ν_{CO} stretch in its IR spectrum similar to one at 1996 cm^{-1} displayed by the enzyme [10].
(5) The metal centers of the M_p–Ni_d unit are coordinatively unsaturated (i.e. with vacant coordination sites) so that such binding of CO and CH_3 can take place and react with organic thiols to form thioester bonds (ACS activity).
(6) One of the Ni centers can be easily removed with chelating ligands like 1,10-phenanthroline (phen).

Clearly, this modeling work involves numerous synthetic challenges. If such a model (or models) can be synthesized, then one can expect that studies on acetylation of a variety of organic thiols with the model complex(es) will provide insight into the mechanisms of the molecular events that occur during acetyl CoA assembly at the A-cluster site in ACS/CODH.

Syntheses of designed thiolate-bridged heterometallic species are however not so trivial. Although Nature often exploits the tendency of thiolato-S to bridge metal centers in assembling multimetallic units such as the one in the A-cluster of ACS/CODH, the extent of bridge formation can hardly be controlled in small molecule systems. As a result, such reactions lead to the formation of S-bridged polymeric species that are insoluble in most solvents and are generally difficult to work with [39]. Researchers often avoid the formation of polymeric species by employing designed ligands that include less electron-rich or sterically hindered thiolates. Careful disposition of the ligand frame around the metal center is also required to form the two sulfur bridges to one metal center as observed in the A-cluster structure. The redox activity of sulfur (coordinated or not) can be an additional problem in the synthesis of such model complexes. Formation of disulfide linkages or sulfur oxygenates (SO_x) requires strict anaerobic conditions during workup [40]. Also, metal-coordinated thiolates are very susceptible to autoredox processes in which the coordinated metal center oxidizes the S-donor(s). Such events lead to the formation of disulfides via thiyl radical(s) and a reduced metal center [41,42]. Collectively, these inherent synthetic difficulties and the structural complexity of the A-cluster pose challenge to the modeling work. However, after the publication of the crystal structure(s) of the A-cluster, modeling activity has gained momentum and over the past 2 years, several papers on A-cluster models have been published. These models are the major focus of this review. A brief report on models synthesized during the pre-ACS/CODH structure period precedes this main topic in the following section.

3.2. Models of ACS/CODH A-cluster: pre-crystal structure period

Although ACS/CODH had been studied by numerous biochemical techniques for quite some time, very few attempts were made at modeling this site before the crystal structure of the *M. thermoacetica* enzyme was determined. Since many researchers at that time believed that the A-cluster site consisted of a mononuclear sulfur-rich Ni site bridged to an Fe_4S_4 cubane (through a Cys-S residue), the modeling attempts focused on relatively simple mononuclear Ni complexes [33,35]. In 1991, Holm and coworkers designed and synthesized a set of mononuclear Ni(II) complexes with the overall goal of creating a functional mimic of the A-cluster [33]. The Ni(II) complexes were derived from the tripodal ligand $NS_3{}^R$ (Fig. 2) containing one amine-N and three thioether-S donors. The chloride-bound complexes, namely $[Ni(NS_3{}^R)Cl](BPh_4)$ (**1**) (where R = ^{i}Pr or ^{t}Bu) serve as viable precursors for the corresponding methyl- and acetyl-bound species (Fig. 2). When green **1** is mixed with the Grignard reagent MeMgCl in THF at −78 °C, the methylated product $[Ni(NS_3{}^R)CH_3](BPh_4)$ (**2**) is rapidly formed as a purple solid (Fig. 2). This diamagnetic product is most easily identified by the characteristic CH_3 resonance of the

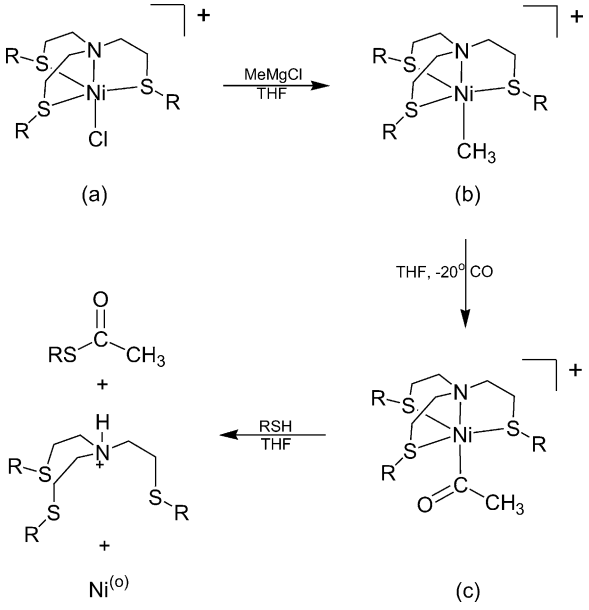

Fig. 2. Reaction sequence for formation of thioesters by Ni^{II} compounds: (a) $[Ni^{II}(NS_3{}^R)Cl]^+$ (cation of **1**); (b) $[Ni^{II}(NS_3{}^R)CH_3]^+$ (cation of **2**); and (c) $[Ni^{II}(NS_3{}^R)COCH_3]^+$ (cation of **3**) where R = ^{i}Pr, ^{t}Bu.

Ni–CH_3 unit at −0.74 ppm (**2** with R = ^{i}Pr) in CD_2Cl_2. In **2** (R = ^{i}Pr), the coordination geometry around the Ni(II) center is distorted trigonal bipyramidal with three thioether-S in the trigonal plane and the amine-N and CH_3 moieties in the axial positions. The N–Ni–C unit is almost linear (177.0°) with a relatively short Ni–C distance of 1.94 Å, somewhat shorter than other known Ni(II)–methyl complexes [43,44]. At the time, complex **2** was one of the very few isolated Ni(II)–CH_3 species that is not supported by strong π-acceptor ligands such as phosphines [43]. In this regard, **2** deserves attention since it contains more biologically relevant S donors and resembles one of the proposed intermediates of ACS/CODH more closely. The insertion of CO into the Ni–C bond of **2** is a facile reaction; passage of CO into a THF solution of **2** at −20 °C results in a rapid color change from purple to red. Workup under CO atmosphere affords the acetylated product $[Ni(NS_3{}^R)COCH_3](BPh_4)$ (**3**) (Fig. 2). The acetyl group of **3** (R = ^{i}Pr) is easily identified by the chemical shift of the $COCH_3$ group (2.32 ppm, CD_2Cl_2) and the ν_{co} stretch (1670 cm^{-1}, KBr) in its IR spectrum. In **3**, the coordination geometry around Ni(II) is distorted trigonal bipyramidal with linear N–Ni–C (179.6°) and bond angles very close to 120° as expected for the sp^2 carbonyl carbon of the Ni–CO–CH_3 unit (118°). Again, isolation of **3** at the time was novel since other known Ni(II)–$COCH_3$ compounds utilized P/As/C ligation [32,45].

Holm and coworkers have also employed the Ni(II)–acetyl complexes (**3**) in acetylation of thiol substrates to demonstrate ACS activity [33]. When thiols (EtSH, PhSH, and $PhCH_2SH$) are added to solutions of **3** in THF, they are converted into the corresponding thioesters (Fig. 2, reaction followed by ^{1}H NMR). The overall yield of thioester is very much dependent on the type of thiol and the R group present on the $NS_3{}^R$ ligand frame. For example, when R = ^{t}Bu, the yields of thioesters are over 95% for all three thiols while with R = ^{i}Pr, the yields are 47, 75 and 80%, respectively after 24 h reaction at room temperature. At the end of the reaction, the formation of a black insoluble residue in the NMR tube indicates formation of elemental Ni. Thus, in the thioester synthesis by **3**, the two electrons required for the reductive elimination of the Ni(II)-bound acetyl group are taken up by Ni(II) (forming Ni(0)) and the proton is captured by the tertiary amine nitrogen of the liberated $NS_3{}^R$ ligand. These reactions are proposed to proceed by direct nucleophilic attack of RSH on the coordinated acetyl carbon with no prior coordination of the RSH species. The reactions of **1**–**3** (Fig. 2) are very noteworthy since they, for the first time, mimicked the steps involved in the assembly of acetyl CoA by ACS/CODH.

In a follow up work, Holm and coworkers have reported another series of Ni(II) complexes with 2,2′-bipyridine (bpy) as the supporting ligand [35]. In this work, they synthesized a preformed green methylated Ni(II) complex, $[Ni(bpy)(CH_3)_2]$ (**4**) [46], and utilized this species to model the ACS reactivity. As shown in Fig. 3, the reaction of **4** with one equiv of RSH (RSH = *p*-toluenethiol, 2,6-dimethylbenzenethiol, mesitylenethiol, 2,4,6-triisopropylbenzenethiol, and 2,6-dichlorobenzenethiol) in THF results in the formation of the purple diamagnetic square planar Ni(II) complex, $[Ni(bpy)(SR)(CH_3)]$ (**5**), with thiolate replacing one CH_3 moiety (Fig. 3). The crystal structure of **5** (with RS^- = 2,6-dichlorobenzenethiolate) reveals a planar Ni(II) center with Ni–C and Ni–S bond distances of 1.921 and 2.149 Å, respectively. The ^{1}H NMR spectrum of **5** (with RS^- = 2,6-dichlorobenzenethiolate) exhibits a resonance of the Ni–CH_3 moiety at −0.28 ppm (THF-d^8). When a THF solution of **5** is exposed to 3 equiv. of CO, an immediate reaction occurs with the formation of a brick-red precipitate. The IR spectrum of the red solid exhibits ν_{co} bands at 1872 and 1973 cm^{-1} (KBr) consistent with the formation of the Ni(0)-dicarbonyl complex $[Ni(bpy)(CO)_2]$ (**7**) (Fig. 3). Analysis of the reaction products by GC/MS and NMR reveals nearly quantitative yields of the thioesters. It is presumed that the formation of thioester and **7** goes through a Ni–$COCH_3$ intermediate as in **3** [33]. Successful isolation of the dark red acetyl species, $[Ni(bpy)(SR)(COCH_3)]$ (**6** with RS^- = 2,6-dichlorobenzenethiolate), is achieved by exposing one equiv of CO to a THF solution of **5** at −5 °C. The ^{1}H NMR spectrum of **6** exhibits a methyl resonance at 2.39 ppm (THF-d^8) and ν_{co} at 1632 cm^{-1} (KBr) in its IR spectrum. Crystallographic studies have confirmed a square planar configuration around Ni(II) in this complex. The Ni–C distance (1.81 Å) in **6** is slightly shorter than that observed in **3** [33]. Also, the relatively short distance between the carbonyl-C and the thiolato-S center (2.82 Å) is noteworthy. This metric feature is presumably responsible for the intramolecular nucleophilic attack of the thiolate group on the $COCH_3$ moiety (bound in *cis* position) leading to the formation of

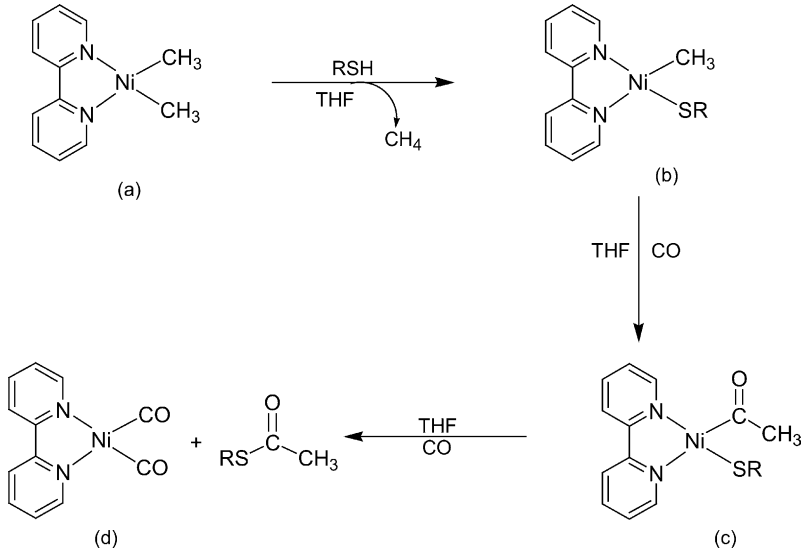

Fig. 3. Reaction sequence for thioester formation by Ni^{II} compounds: (a) [Ni^{II}(bpy)$(CH_3)_2$] (**4**); (b) [Ni^{II}(bpy)(SR)(CH_3)] (**5**); (c) [Ni^{II}(bpy)(SR)$(COCH_3)$] (**6**); and (d) [Ni^{0}(bpy)$(CO)_2$] (**7**) where RS^- = anion of *p*-toluenethiol, 2,6-dimethylbenzenethiol, mesitylenethiol, 2,4,6-triisopropylbenzenethiol, and 2,6-dichlorobenzenethiol.

thioester. The mechanism of thioester synthesis mediated by Ni(II)–bpy complexes in Fig. 3 therefore differs from the nucleophilic attack of free RSH on the Ni(II)-bound $COCH_3$ moiety in case of the Ni(II)–NS_3^R complexes **1**–**3** (Fig. 2). Although, both these earlier model systems (**1**–**3** and **4**–**7**) are structurally quite distinct from the ACS active site, their reactivities demonstrate that thioester synthesis can occur at Ni(II) centers by two separate pathways and such pathways could very well be involved in the formation of acetyl CoA by ACS/CODH.

More recently, Riordan and coworkers have reported the syntheses and isolation of Ni(I) complexes based on a tripodal thioether ligand [47–49]. When the Tl^+ salt of $PhTt^{tBu}$ in CH_2Cl_2 is mixed with a methanolic solution of $[Ni(H_2O)_6]Cl_2$, the red Ni(II) complex [($PhTt^{tBu}$)Ni(Cl)] (**8**) is formed in good yield (Fig. 4) [47]. The geometry around the Ni(II) center in **8** is distorted tetrahedral with the three *tert*-butyl thioether S atoms ligated to Ni in a facial array. This arrangement gives rise to a three-fold symmetry along the Ni(II)–Cl bond. Spectroscopic data, consistent with the structure, indicate an S = 1 ground state (solution magnetic moment: 2.5 μ_B) and well-resolved contact-shifted ^{1}H NMR resonances are noted for the ligand protons in **8**. In CH_2Cl_2, **8** exhibits an irreversible reduction wave at −1.302 V (versus Fc^+/Fc). Reduction of **8** with Na/Hg amalgam in THF affords an air-sensitive brown compound that displays a rhombic EPR spectrum with g values = 2.40, 2.18, 2.12 (THF, 77 K). Furthermore, when **8** is reduced with CH_3Li in THF at −78 °C under CO atmosphere, the corresponding orange CO-adduct, [($PhTt^{tBu}$)Ni(CO)] (**9**), is formed (Fig. 4) [48]. As in **8**, the Ni(I) center in **9** is distorted tetrahedral with the Ni–CO bond along the molecular three-fold axis (Ni–C–O angle: 171.0°). The average Ni–S and Ni–C bond distances in **9** are 2.24 and 1.754 Å, respectively. The IR spectrum (KBr) of **9** contains one strong ν_{CO} band at 1999 cm^{-1} consistent with terminal CO ligation. It is interesting to note that this ν_{CO} value matches very well with the ν_{CO} value (1996 cm^{-1}) of the CO-bound form of ACS/CODH which is also proposed to contain a Ni(I)–CO unit [10]. In toluene glass (4.2 K), **9** displays a rhombic EPR signal with significant axial character (g = 2.64, 2.02, and 1.95) [49]. Comparison of the EPR spectrum of **9** with the NiFeC signal of the ACS A-cluster shows significant electronic differences between the two Ni sites. Nevertheless, results of spectroscopic and computational studies on **9** have revealed that extensive Ni(I) → CO π-back-bonding interaction is responsible for the low ν_{CO} stretching frequency (also true for ACS). Such back-bonding induces significant nucleophilic character at the Ni(I) center required for the methyl transfer step [49]. Furthermore, the EPR results strongly suggest that the coordination geometry at the Ni(I) site in the enzyme is either trigonal bipyramidal or tetragonally elongated octahedral when CO is bound [49].

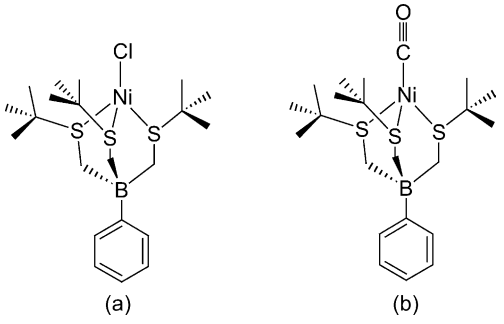

Fig. 4. Structures of (a) [($PhTt^{tBu}$)Ni^{II}(Cl)] (**8**) and (b) [($PhTt^{tBu}$)Ni^{I}(CO)] (**9**).

3.3. Models of ACS/CODH A-cluster: post-crystal structure period

3.3.1. Ni_d site models

Although the structural characterization of the ACS site has been completed only recently, a small number of complexes that mimic the Ni_d dicarboxamido-dithiolato site to a remarkable extent did exist prior to the crystallographic study. These monomeric Ni(II) complexes with dicarboxamido-dithiolato (N_2S_2) coordination sphere were synthesized by different groups for different purposes (Fig. 5) [50–57]. For example, in the late 1980s and early 1990s, Holm and coworkers synthesized many of these NiN_2S_2 complexes as analogues for the Ni site in the NiFe hydrogenases [50,51]. Interestingly, complexes like **10**–**13** (Fig. 5a–d) do serve as appropriate structural models for the Ni_d site in the A-cluster of ACS/CODH. These complexes were prepared by mixing the N_2S_2 ligands with $Ni(OAc)_2{\cdot}4H_2O$ in methanol under basic conditions and were isolated as their Et_4N^+ salts in good yields. Complexes **10**–**13** are all square planar and diamagnetic. The metric parameters of these complexes are quite similar to each other. For example, average Ni–N distances in **10** (structurally characterized by Murray and coworkers [52]) and **11** are 1.90 and 1.86 Å, respectively. In ethanol, the complexes exhibit red to red-orange color due to two sets of d–d bands around 540 and 435 nm. Another interesting feature of the complexes **10**–**13** is their relatively low $E_{1/2}$ value for the Ni(II)/Ni(III) redox couple. For example, in DMF, **11** and **13** exhibit reversible cyclic voltammograms with $E_{1/2}$ values at −0.34 and −0.42 V (versus SCE), respectively. The potentials of **10**–**13** are among the lowest values of the Ni(II)/Ni(III) couple noted for small model complexes. Typically, the Ni(III) species (formed in situ) exhibit blue-violet color and are readily identified by EPR spectroscopy. The Ni(III) species derived from **11** exhibits a rhombic EPR spectrum in DMF glass (77 K) with $g = 2.226$, 2.181, and 2.007.

In 1998, Krüger and coworkers synthesized an analogous Ni(II) complex $(PPh_4)_2$[Ni(phmi)] (**14**) (Fig. 5e) as part of

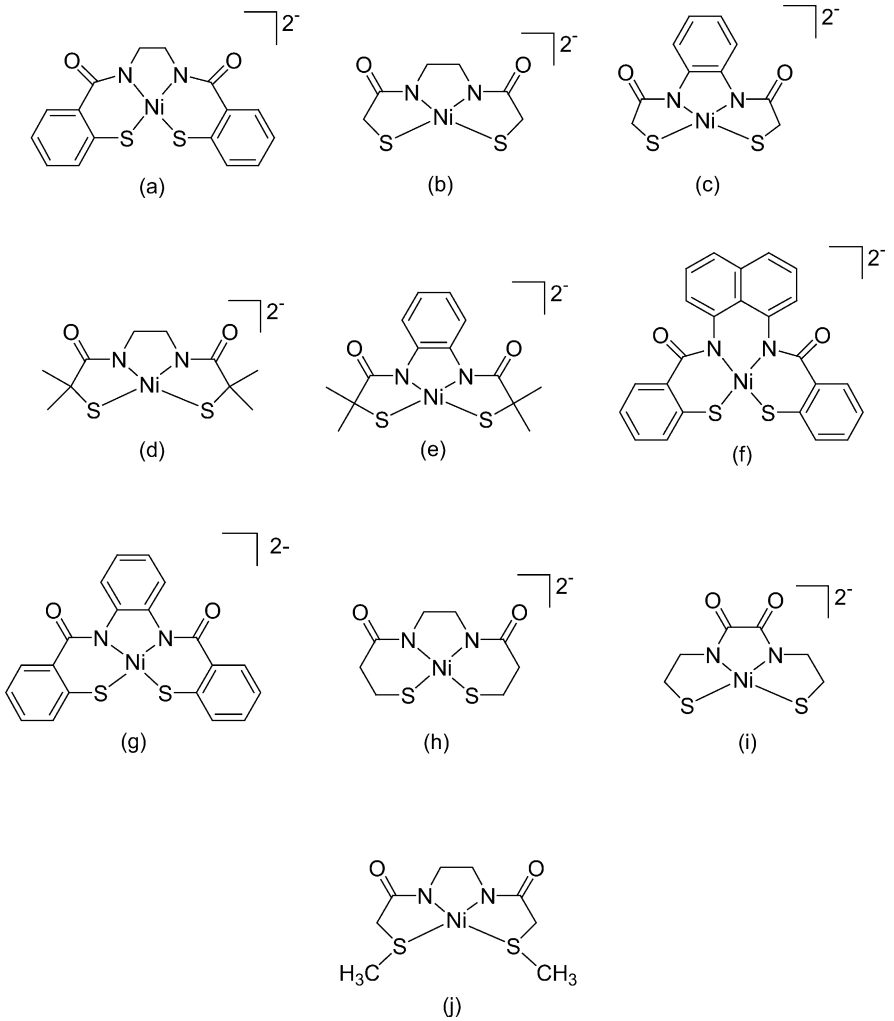

Fig. 5. Structures of Ni(II)-dicarboxamido-dithiolato complexes: (a) $[Ni^{II}(emb)]^{2-}$ (anion of **10**); (b) $[Ni^{II}(ema)]^{2-}$ (anion of **11**); (c) $[Ni^{II}(phma)]^{2-}$ (anion of **12**); (d) $[Ni^{II}(emi)]^{2-}$ (anion of **13**); (e) $[Ni^{II}(phmi)]^{2-}$ (anion of **14**); (f) $[Ni^{II}(NpPepS)]^{2-}$ (anion of **15**); (g) $[Ni^{II}(PhPepS)]^{2-}$ (anion of **16**); (h) $[Ni^{II}(S_2N'_2)]^{2-}$ (anion of **17**); (i) $[Ni^{II}(N,N'$-bis(2-mercaptoethyl)oxamide$)]^{2-}$ (anion of **18**); (j) $[Ni^{II}(N,N'$-ethylenebis(2-methylmercaptoacetamide$))]$ (**19**).

their research in the area of Ni-hydrogenase modeling [53]. In MeCN, this orange-red diamagnetic square planar complex displays d–d bands at 550 and 430 nm. As expected, the metric and redox parameters of **14** are very similar to those of **10** and **13**. The corresponding Ni(III) species (PPh_4)[Ni(phmi)], synthesized via electrolytic oxidation of **14**, has also been isolated and structurally characterized. Although the square planar coordination environment remains unchanged, both the Ni–N and Ni–S bond lengths are reduced upon oxidation. In solid state, (PPh_4)[Ni(phmi)] exhibits a somewhat broad rhombic EPR signal with apparent g values of 2.55, 2.14 and 2.00.

Mascharak and coworkers have synthesized two square planar air-stable Ni(II) complexes, namely $(Et_4N)_2$[Ni(NpPepS)] (**15**) and $(Et_4N)_2$[Ni(PhPepS)] (**16**) (Fig. 5f and g) from $(Et_4N)_2[NiCl_4]$ and the mixed carboxamido-N/thiolato-S donor ligands $NpPepS^{4-}$ and $PhPepS^{4-}$, respectively, in DMF [54,55]. The electronic absorption spectrum of **15** contains several features responsible for the dark red color including a d–d band at 550 nm and two π–π* bands at 460 and 420 nm in DMF solution. Complex **16** exhibits its d–d band at 545 nm and π–π* bands at 384 and 331 nm in MeCN. The $NpPepS^{4-}$ ligand in **15** wraps around the Ni(II) center in an unusual "butterfly" fold of the aryl sulfur rings forming a hydrophobic pocket on one side of the NiN_2S_2 plane [54]. Due to the decreased steric demand imposed by the $PhPepS^{4-}$ ligand frame, this "butterfly" fold is less prominent in complex **16** [55]. The average Ni–N and Ni–S distances of **15** (1.91 and 2.17 Å, respectively) and **16** (1.91 and 2.16 Å, respectively) are similar to those noted for **10**–**14**. In DMF, **15** and **16** display irreversible metal-centered oxidation waves at 0.13 and 0.22 V, respectively versus SCE. The weaker donor strength of the aryl thiolates in **15** and **16** compared to that of the alkyl thiolates in **11** and **13** is presumably responsible for the more positive Ni(II)/Ni(III) potential. Not surprisingly, both **15** and **16** show no reduction wave up to a potential of −1.8 V versus SCE (in DMF) due to the presence of strong σ donors (carboxamido-N and thiolato-S) around the Ni(II) center.

Recently, Hegg and coworkers have synthesized a series of NiN_2S_2 complexes specifically for modeling the Ni_d site in ACS/CODH [56]. Reaction of $Ni(OAc)_2{\cdot}4H_2O$ with the deprotonated ligands in basic methanol affords the NiN_2S_2 complexes **17** and **18** (Fig. 5h and i) in good yields. Complex **17** was originally synthesized and structurally characterized by Rauchfuss and coworkers [57]. In MeCN, these two diamagnetic square planar complexes exhibit d–d bands at 550 and ∼440 nm and are irreversibly oxidized at −0.43 and −0.40 V (versus SCE), respectively. Hegg and coworkers have also reported a thioether complex [Ni(*N*,*N*′-ethylenebis(2-methylmercaptoacetamide))] (**19**, Fig. 5j) synthesized via methylation of **11** with CH_3I in MeCN [56]. The metric parameters of neutral yellowish orange complex **19** (average Ni–N and Ni–S distances of 1.84 and 2.19 Å, respectively) [56] do not differ much from the parent thiolato species **11** [51]. Since the thiolato sulfurs of the Ni_d site of the A-cluster bridge the M_p metal, it was thought that methylation of **11** to form **19** would afford a more accurate electronic mimic of the Ni_d site. Indeed, Darensbourg and coworkers have shown that methylation, metallation, or oxygenation of Ni(II)-bound thiolato-S centers can effectively neutralize the electronic charge on sulfur, altering the electronic properties of the resulting complexes [40,58,59]. The main difference between the thioether complex **19** and the thiolato complexes **10**–**18** lies in the electrochemical properties. Upon charge neutralization of thiolato-S centers to thioether in **19**, the Ni(II)/Ni(III) couple shifts to more positive value of 1.0 V versus SCE (MeCN). Also, the Ni(I)/Ni(II) couple is now accessible in **19** with a quasireversible wave centered at −1.50 V versus SCE (MeCN). The high negative $E_{1/2}$ value however suggests that it is still very difficult to reduce **19**. Collectively, the electrochemical properties of **10**–**19** indicate that the Ni_d site is highly resistant to reduction and hence is *not* expected to participate in the catalytic cycle as Ni(I) [4,11].

In addition to structural similarities to the Ni_d site of the A-cluster, complexes **10**–**19** exhibit several common spectroscopic and redox features that provide insight into the possible role of Ni_d in the overall ACS activity. These models (i) exist exclusively in square planar geometry affording diamagnetic d^8 metal centers, (ii) afford red to red-orange solutions due to absorption bands in the 530–570 and 430–460 nm range, (iii) display Ni–N_{amido} distances in the range of 1.86–1.94 Å and Ni–S distances in the range of 2.16–2.19 Å, (iv) are very resistant to reduction with no observable reduction up to −1.8 V versus SCE [60], (v) are easily oxidized at low E_{ox} values for the Ni(II/III) couple ranging from −0.42 to 0.22 V, (vi) show no affinity toward binding additional ligand(s) in axial position(s), and (vii) are generally stable in presence of O_2. Any proposed mechanism of acetyl coenzyme A synthesis must take these features into consideration. Indeed, these features have already raised question regarding the mechanism that includes addition of CH_3^+ to the Ni_d center with Ni in +1 oxidation state [4,20]; reduction of the Ni_d site appears highly unlikely on the basis of the redox properties of all the models of the Ni_d sites reported so far.

3.3.2. *Higher nuclearity Cu_p–Ni_d models*

To date, the most common approach employed in modeling the A-cluster of ACS has been to ignore the Fe_4S_4 cubane, since it is an unlikely site for CO or CH_3 binding. The synthetic efforts have been directed mostly toward the design and isolation of models that mimic the thiolato-bridged bimetallic M_p–Ni_d subsite. A general synthetic route to these models involves the reaction of mononuclear Ni(II)-di-carboxamido/amine-dithiolato metallosynthons (Ni_d models) with appropriate mononuclear ML_n fragments containing labile ligands to build the binuclear complex required for modeling the bimetallic portion of the ACS active site (Scheme 2).

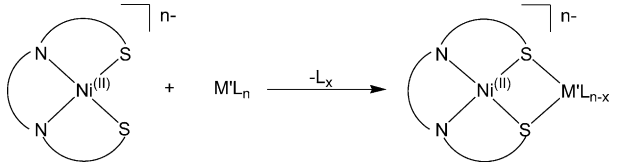

Scheme 2.

Since the first structure of ACS/CODH reported by Drennan and coworkers revealed a Cu(I) ion at the proximal metal site (M_p) [4], several groups attempted the syntheses of models containing sulfur-bridged Cu–Ni moieties. In one of the first accounts of synthetic modeling of this unique site (post-crystal structure period), Riordan and coworkers employed both Ni(II)-diamino-dithiolato and Ni(II)-dicarboxamido-dithiolato units as metallosulfur ligands for Cu(I) centers [61]. These initial attempts provided insight into the difficulties associated with the synthesis of such units. First, reaction of simple Cu(I) salts such as $[Cu(MeCN)_4]^+$ with the NiN_2S_2 units in MeCN resulted in the polynuclear species, $[\{(EtN_2S_2)Ni\}_3Cu_2](BF_4)_2$ (**20**) and $K_2[\{(phmi)Ni\}_2Cu_2]$ (**21**), with each thiolate donor within the same ligand frame coordinated to different Cu(I) centers rather than chelating only one Cu(I) ion (Fig. 6). The formation of such polynuclear species has been attributed to the steric demands imposed by the aliphatic ligand frame(s). Later, this group was able to isolate the desired thiolato-bridged Cu–Ni complexes, namely $[(EtN_2S_2)NiCu(PhTt^{tBu})]$ (**22**) and $K_2[Ni(phmi)Cu(PhTt^{tBu})]$ (**23**) (Fig. 6) by changing the Cu(I) source to the less labile complex $[Cu(PhTt^{tBu})(MeCN)]$ [62]. In **22**, the starting Cu(I) complex loses one MeCN molecule and one thioether S donor to allow the bridging of two metallothiolate ligands from the NiN_2S_2 units to the Cu(I) center. The resulting coordination environment of two bridging thiolates and two thioether sulfurs around the Cu(I) centers in both **22** and **23** is very similar to that in the enzyme. The Cu–S distances in **22** give rise to an asymmetric and distorted Cu(I) center much like that in the enzyme [4]. The Ni–Cu distance in **22** (2.917 Å) is slightly longer than that in the A-cluster (2.79 Å). Both complexes exhibit redox parameters associated with the ligand or the Ni centers. No oxidation of the Cu(I) centers in these complexes is apparent. Interestingly, the Ni(II) centers coordinated to carboxamido-N in **21** and **23** show no reduction wave, a fact that once again indicates a non-redox role of the Ni_d center of the A-cluster. Although the complexes with amine nitrogen bound to Ni(II) display a reduction wave (for the Ni(I)/Ni(II) couple), the potentials are highly negative (close to −2 V versus NHE) and hence are hardly accessible in biological systems. Bubbling of CO through solutions of **22** and **23** results in the rupture of the thiolate bridges affording the respective NiN_2S_2 units and the CO-adduct $[Cu(PhTt^{tBu})(CO)]$ (ν_{co} at 2078 cm^{-1}). No reaction is observed with CO and **21**. Curiously, **20** reacts with CO to afford a CO-adduct with a terminal M–CO bond (ν_{co} at 2042 cm^{-1}). However, the identity of this species has not been established yet.

Rauchfuss and coworkers have also employed simple Cu(I) salts and NiN_2S_2 units to synthesize Cu–Ni models [57]. The results are quite similar to those obtained by Riordan's group. For example, the reaction of $[Cu(MeCN)_4]^+$ with a diamino NiN_2S_2 unit in MeCN resulted in the formation of the polynuclear complex, $[Cu_2\{Ni(S_2N_2)\}_2](BF_4)_2$ (**24**, Fig. 7), that adopts a staircase structure similar to **21** [61]. However, this polynuclear complex can be

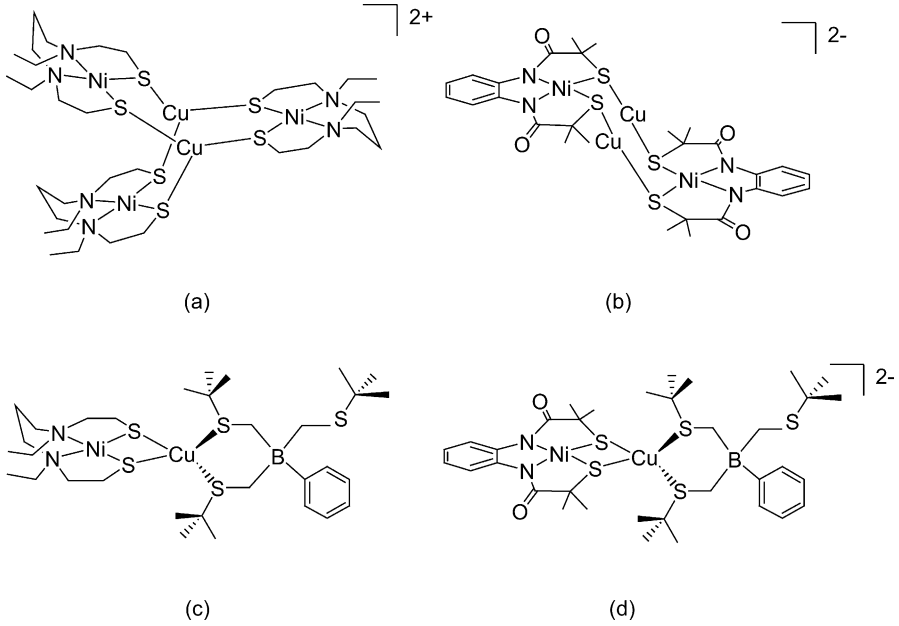

Fig. 6. Structures of: (a) $[\{(EtN_2S_2)Ni^{II}\}_3Cu^I_2]^{2+}$ (cation of **20**); (b) $[\{(phmi)Ni^{II}\}_2Cu^I_2]^{2-}$ (anion of **21**); (c) $[(EtN_2S_2)Ni^{II}Cu^I(PhTt^{tBu})]$ (**22**); and (d) $[Ni^{II}(phmi)Cu^I(PhTt^{tBu})]^{2-}$ (anion of **23**).

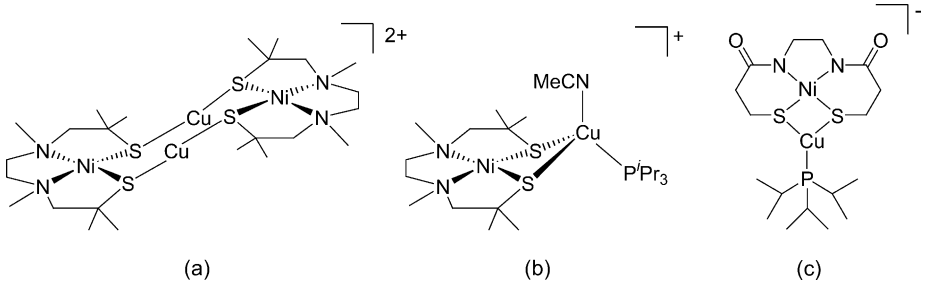

Fig. 7. Structures of: (a) $[Cu^{I}_2\{Ni^{II}(S_2N_2)\}_2]^{2+}$ (cation of **24**); (b) $[\{(P^iPr_3)(NCMe)Cu^{I}\}\{Ni^{II}(S_2N_2)\}]^{+}$ (cation of **25**); (c) $[\{(P^iPr_3)Cu^{I}\}\{Ni^{II}S_2N'_2\}]^{-}$ (anion of **26**).

broken down through addition of triisopropylphosphine to afford the thiolate-bridged binuclear Cu–Ni complex $[\{(P^iPr_3)(NCMe)Cu\}\{Ni(S_2N_2)\}](PF_6)$ (**25**) (Fig. 7) that contains a distorted Cu(I) ion with a labile MeCN ligand. In addition to this Cu–Ni model, this group has also reported a second complex, $(Et_4N)[\{Cu(P^iPr_3)\}(NiS_2N'_2)]^{-}$ (**26**) in which the dicarboxamido complex **17** is bridged to a planar three-coordinate Cu(I) ion (Fig. 7). The Ni–Cu distance in **26** is 2.672 Å, slightly shorter than that observed in the enzyme (2.79 Å). The absence of a fourth ligand at the Cu(I) center in **26** presumably reflects the enhanced donor power of the dicarboxamido NiN_2S_2 unit which provides enough electron density to the Cu(I) center to give rise to a three-coordinate unsaturated site. Although the Cu(I) center in **26** is not easily oxidized, the Ni(II) center undergoes irreversible oxidation at 0.18 V versus Ag/AgCl in MeCN. However, no reduction of the Ni center is observed with this model. Unlike **20**–**23**, the complexes reported by Rauchfuss and coworkers (**24**–**26**) do not react with CO. It is interesting to note that the coordinatively unsaturated Cu(I) center of **26** does not exhibit any affinity toward CO despite coordinative unsaturation. This strongly suggests that CO may not bind to the M_p site of the enzyme if occupied by Cu(I).

In a series of papers, Darensbourg and coworkers have reported the syntheses, structural characterization, and properties of a variety of polymetallic complexes based on the well characterized [(BME-DACO)Ni] complex [60]. For instance, reaction of $NiBr_2$ with [(BME-DACO)Ni] in methanol results in the formation of red-brown trimeric $[\{(BME\text{-}DACO)Ni\}_2Ni]Br_2$ (**27**) where two [(BME-DACO)Ni] units serve as a bidentate chelating ligand to a single Ni(II) ion in square planar geometry (Fig. 8) [63]. In **27**, the familiar stepped structure is noted with average Ni–S distance of 2.20 Å at the central NiS_4 unit. The Ni–Ni separation in **27** is 2.69 Å, similar to that observed in other trimetallic Ni complexes [64]. Not much change is observed in the metric parameters of the NiN_2S_2 units of **27** compared to [(BME-DACO)Ni]. Only slight shortening of the Ni–N distance (1.96 Å in **27** versus 1.99 Å in [(BME-DACO)Ni]) is noted upon S-metalation. The electronic absorption spectrum of **27** in ethanol exhibits charge transfer bands (LMCT) at 486 and 408 nm and one d–d band at 564 nm. As expected, upon S-metalation, the Ni(III) state in **27** is less accessible with respect to [(BME-DACO)Ni] (E_{ox} = 1.10 and 0.36 V versus NHE in H_2O for **27** and [(BME-DACO)Ni], respectively). Along the same line, the +1 oxidation state is more accessible in **27** ($E_{1/2}$ = −0.71 and −1.94 V versus NHE in H_2O for **27** and [(BME-DACO)Ni], respectively) [59]. The reduction of the terminal NiN_2S_2 units in **27** can be easily followed by EPR spectroscopy; an axial signal, consistent with Ni(I) in tetrahedral geometry is observed upon reduction [59]. Interestingly, reaction of [(BME-DACO)Ni] with anhydrous $ZnCl_2$ in MeOH affords the red complex $[\{(BME\text{-}DACO)Ni\}_3Zn_2Cl_2](BF_4)_2$ (**28**) regardless of stoichiometry. In **28**, the [(BME-DACO)Ni] unit acts as a bidentate bridging ligand to two separate Zn(II) centers in distorted tetrahedral geometry (Fig. 8) [65]. The average Zn–S distance and S–Zn–S angle in **28** are 2.35 Å and 112°, respectively. The heterometallic complex **28** is not stable in protic media and decomposes readily into [(BME-DACO)Ni] units and solvated Zn^{2+} ions. In MeCN, **28** exhibits an irreversible Ni(II)/Ni(III) wave at 0.50 V versus Ag^{+}/AgCl. In addition, two reversible reductions at $E_{1/2}$ = −1.03 and −1.25 V and an irreversible event at −1.45 V (all versus Ag^{+}/AgCl in MeCN) are also observed. These reductions are assumed to be sequential reductions of the three NiN_2S_2 units to the Ni(I) oxidation state [65]. It is important to note at this point that even though these models employ NiN_2S_2 units bearing amine-N donors (versus carboxamido-N donors in ACS/CODH), the reduction potentials are still very high.

In a recent paper, Darensbourg and coworkers have also reported the Cu(I)–Ni(II) heterobimetallic model $[\{(BME\text{-}DACO)Ni\}_3Cu_2Br_2]$ (**29**) and reexamined the metal ion binding affinity of the [(BME-DACO)Ni] unit in relation to the discovery of different metal ions at the ACS/CODH structure [66]. Reaction of CuBr with [(BME-DACO)Ni] in MeCN affords the yellow-brown polymetallic complex **29** that is nearly isostructural with **28** (Fig. 8). While the complexes **27**–**29** are not exact structural analogues of the M_p–Ni_d bimetallic site in ACS/CODH, their reactions (Fig. 8) reveal the relative affinity of the terminal thiolates of the NiN_2S_2 unit toward other metal ions. The results of the competition experiments (monitored by electronic absorption spectroscopy in MeOH) clearly show that both Ni(II) and Cu(I) can displace Zn(II) in complex **28**. In contrast, Zn(II) cannot displace Ni(II) or Cu(I) form complexes **27** and

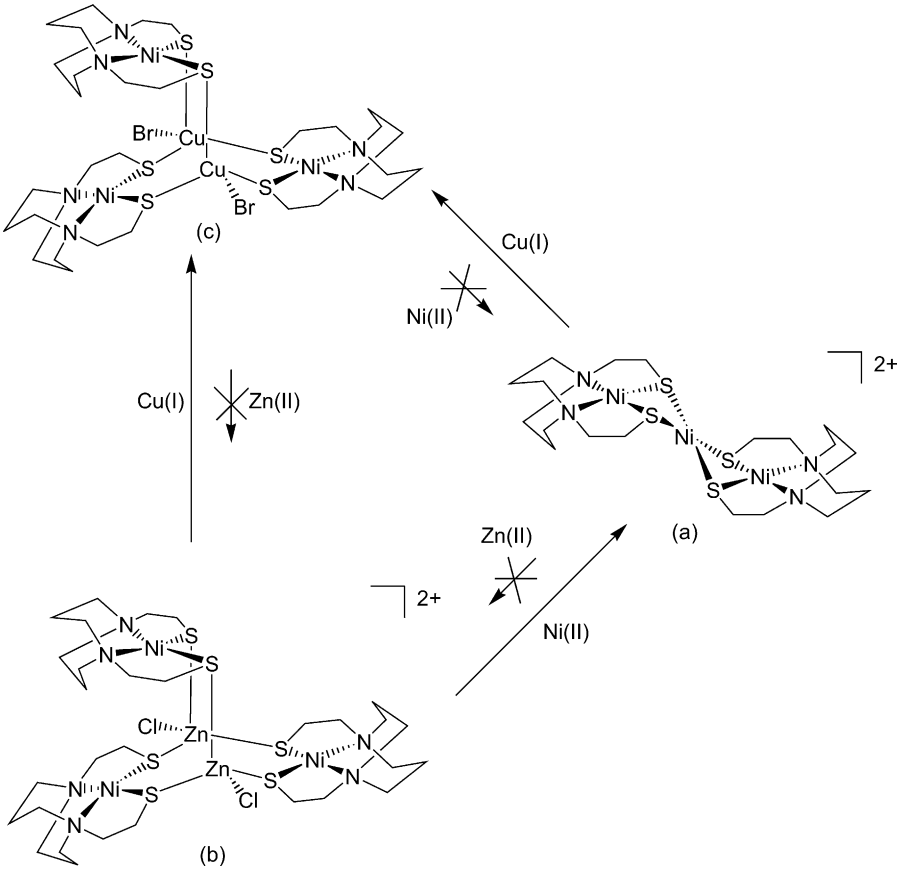

Fig. 8. Metal ion exchange in polymetallic complexes: (a) $[\{(BME\text{-}DACO)Ni^{II}\}_2Ni^{II}]^{2+}$ (cation of **27**); (b) $[\{(BME\text{-}DACO)Ni^{II}\}_3Zn^{II}_2Cl_2]^{2+}$ (cation of **28**); (c) $[\{(BME\text{-}DACO)Ni^{II}\}_3Cu^{I}_2Br_2]$ (**29**).

29, respectively. Also, while no reaction is observed with the Cu–Ni complex **29** with $NiCl_2$, CuBr readily reacts with the trimeric complexes **27** and **28** to afford **29**. Thus the metal ion affinity of the metallothiolate sulfurs of [(BME-DACO)Ni] is Cu(I) > Ni(II) > Zn(II). Darensbourg and coworkers have also shown that the central Ni(II) center in **27** can be removed with 3 equiv. of phen to afford $[Ni(phen)_3]^{2+}$ and [(BME-DACO)Ni]. No further change is observed upon addition of excess phen (up to 6 equiv.) to the reaction mixture. It is therefore evident that the 'labile Ni' observed in the enzyme comes from Ni(II) present at the M_p site but not from the Ni_d site. Also, the facile replacement of the Ni(II) center by Cu(I) could explain the presence of Cu(I) at the M_p site in the Drennan structure [4]. Since such replacement leads to inactivation of the ACS site [12,21], the Ni_p–Ni_d description of the catalytically active ACS site appears more reasonable.

Mascharak and coworkers have employed the dicarboxamido $[Ni(NpPepS)]^{2-}$ unit (anion of **15**) to make higher nuclearity complexes with Cu(I) [67]. Reaction of CuCl with **15** in solvents like DMF or MeCN results in the formation of the trinuclear complex $(Et_4N)_3[Cu\{Ni(NpPepS)\}_2]$ (**30**), regardless of the NiN_2S_2/Cu(I) stoichiometry (Fig. 9). Unlike the previous reports, no polymeric S-bridged species is formed and **30** is the only product in such reactions. The

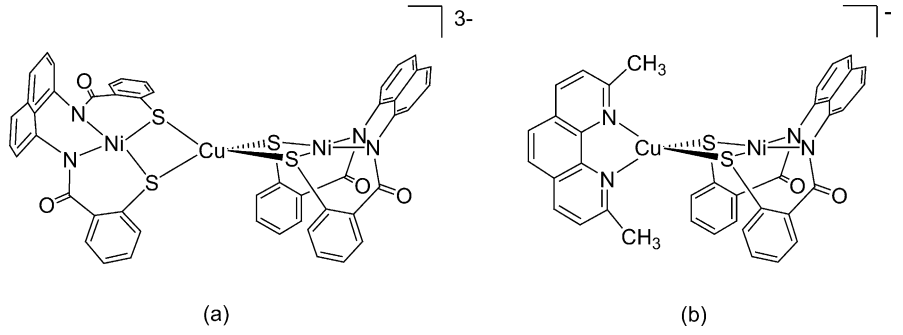

Fig. 9. Structures of: (a) $[Cu^{I}\{Ni^{II}(NpPepS)\}_2]^{3-}$ (anion of **30**) and (b) $[Cu^{I}(neo)Ni^{II}(NpPepS)]^{-}$ (anion of **31**).

geometry around Cu(I) in **30** is distorted tetrahedral and the Ni–Cu distance (3.24 Å) is longer than that observed in the enzyme. The central Cu(I) center in **30** is bound to four metallosulfur ligands (versus three $Cu–S_{Cys}$ in ACS) and is not removable by phen. It is however readily removed by neocuproine (neo). Addition of neo to **30** in DMF readily affords **15** and $[Cu(neo)_2]^+$. The Cu(I) ion in Cu-ACS is also labile and can be removed with neo but not phen [21]. In this regard, the Cu(I) center in **30** mimics the Cu_p site in the Cu-containing ACS. Mascharak and coworkers have also synthesized a binuclear Cu–Ni model in which neo serves as one of the ligands of the bridged Cu(I) center. Reaction of **15** with [Cu(neo)Cl] in MeCN affords (Et_4N)[Cu(neo)Ni(NpPepS)] (**31**) (Fig. 9) [55]. The Ni–Cu distance of **31** (3.074 Å) is noticeably shorter than that of **30** presumably due to the steric demands of two units of **15** bound to Cu(I) in **30**. Both **30** and **31** exhibit no reduction of the Ni(II) centers (up to −1.8 V versus SCE in DMF) and like most reported Cu–Ni models exhibit no reactivity toward CO. No breakdown of the sulfur bridges is observed in reactions of these two models with CO. It is important to note here that even **26**, the Cu–Ni model with coordinatively unsaturated Cu(I) center, does not react with CO [57]. The consistent lack of reactivity of the various Cu–Ni models toward CO strongly suggests that Cu(I) centers in metallosulfur coordination environment does not bind CO. This in turn provides support to the notion that Cu(I) is not the catalytically active metal at the proximal site in the A-cluster of ACS/CODH. Indeed, recent results of studies on the enzyme indicate that Cu serves a deleterious non-catalytic role in ACS/CODH while the presence of Ni at the M_p site activates the enzyme [12,21].

3.3.3. *Higher nuclearity Ni_p–Ni_d models*

Rauchfuss and coworkers have reported the first binuclear Ni complexes with NiN_2S_2 units bearing carboxamide donors [57]. The mixed valence complex $(Et_4N)_2[\{Ni(CO)_2\}\{NiS_2N'_2\}]$ (**32**) (Fig. 10) was synthesized by treatment of **17** with $[Ni(cod)_2]$ at −40 °C in MeCN/toluene followed by mild carbonylation (1 atm, 20 min, −5 °C). The geometry around the Ni(II) center in

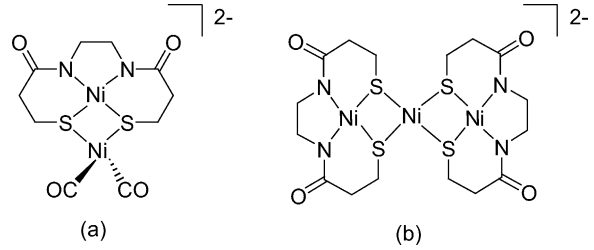

Fig. 10. Structures of: (a) $[\{Ni^0(CO)_2\}\{Ni^{II}S_2N'_2\}]^{2-}$ (anion of **32**) and (b) $[Ni^{II}\{Ni^{II}S_2N'_2\}_2]^{2-}$ (anion of **33**).

32 is square planar while the Ni(0) center resides in a tetrahedral geometry. In MeCN solution, **32** displays strong ν_{CO} bands at 1948 and 1866 cm^{-1} consistent with terminally bound Ni(0)–CO species. This Ni(II)–Ni(0) complex is stable only under anaerobic atmosphere; exposure of **32** to air results in oxidative degradation leading to the trimeric species, $(Et_4N)_2[Ni\{NiS_2N'_2\}_2]$ (**33**) with the typical step structure (Fig. 10). Addition of PPh_3 to a solution of **32** removes the Ni(0) center to form $[Ni(PPh_3)_2(CO)_2]$. Although participation of Ni(0) in the ACS mechanism is still questionable, complex **32** is the first structurally characterized example of a sulfur-bridged Ni–Ni model with terminally bound CO molecule(s).

Riordan and coworkers have employed a Cys-Gly-Cys tripeptide complex of Ni(II) namely K_2[Ni(CGC)] (**34**) as metallosynthon to build polynuclear model complexes (Fig. 11) [68]. Reaction of **34** with simple Ni(II) salts like $[Ni(H_2O)_6]Cl_2$ in aqueous solution results in formation of green trinuclear $K_2[\{Ni(CGC)\}_2Ni]$ (**35**) (Fig. 11). Complex **35** is diamagnetic, consistent with square planar metal centers. Also, **35** displays a reversible reduction at −0.995 V (versus NHE) assigned to the Ni(II) centers of the outer two NiN_2S_2 units. No reaction with CO has been reported with **35**. The metallosynthon **34** has also been utilized in the synthesis of Ni–Ni models. Reaction of $[Ni(dRpe)Cl_2]$ (where R = Et or Ph) with K_2[Ni(CGC)] in DMF results in the formation of deep red [Ni(CGC)Ni(dRpe)] (**36**) in good yield (Fig. 11). This species is also diamagnetic, consistent with a planar NiP_2S_2 bridged unit. Unfortunately, none of these

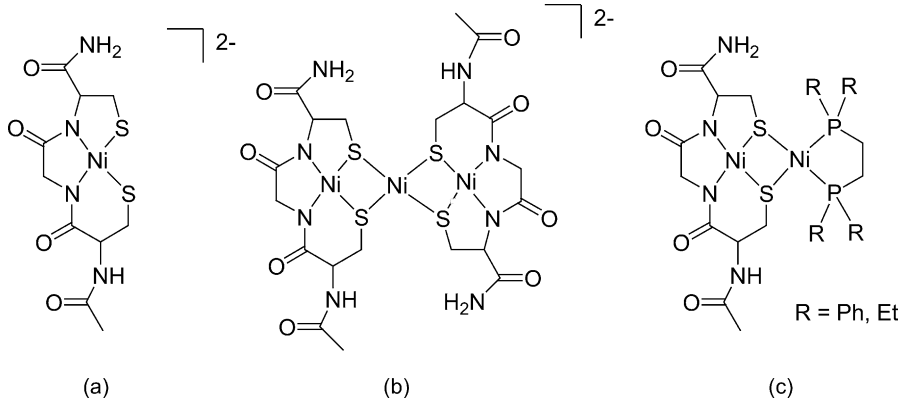

Fig. 11. Structures of: (a) $[Ni^{II}(CGC)]^{2-}$ (anion of **34**); (b) $[\{Ni^{II}(CGC)\}_2Ni^{II}]^{2-}$ (anion of **35**); and (c) $[Ni^{II}(CGC)Ni^{II}(dRpe)]$ (**36**).

species (**34**–**36**) has been characterized by crystallography. Also, the presence of additional peptide moieties in the CGC ligand frame makes assignment of the structures (as shown in Fig. 11) rather ambiguous. Both $\mathbf{36}^{Ph}$ and $\mathbf{36}^{Et}$ display two one-electron reduction processes, a reversible one in the range −0.5 to −0.8 V and a second quasireversible one in the range −1.3 to −1.6 V (both versus NHE in MeCN). The first reduction has been assigned to the NiP_2S_2 unit in **36**. The higher reduction potential for $\mathbf{36}^{Et}$ (−0.828 V) is in accord with the greater donor ability of dialkyl phosphines versus diphenyl phosphines (−0.531 V for $\mathbf{36}^{Ph}$). Although $\mathbf{36}^{Ph}$ and $\mathbf{36}^{Et}$ display no affinity for CO in the oxidized states, minor shifts of the reduction waves under CO atmosphere suggest that the reduced forms might bind CO [68]. Interestingly, the cathodic event under CO atmosphere indicates the occurrence of a two-electron process. Riordan and coworkers have proposed that the CO binding occurs in a three-step process that involves (a) reduction of the $Ni^{II}Ni^{II}$ unit of **36** to $Ni^{II}Ni^{I}$, (b) CO binding to the one-electron reduced species generating $Ni^{II}Ni^{I}$–CO, and (c) the final reduction of $Ni^{II}Ni^{I}$–CO to $Ni^{II}Ni^{0}$–CO. Although the CO-bound species have not been characterized by any spectroscopic or structural studies, the redox behavior of $\mathbf{36}^{Ph}$ and $\mathbf{36}^{Et}$ under CO demonstrates that reduction of the bridged Ni(II) center could facilitate CO binding.

Schröder and coworkers have structurally characterized an asymmetric binuclear Ni(II) model that contains a chelating phosphine as one ligand [69]. Reaction of [Ni(L)], where L = *N*,*N*′-diethyl-3,7-diazanonane-1,9-dithiolate^{2-}, with $[Ni(dppe)Cl_2]$ in MeCN affords red $[(dppe)Ni(\mu\text{-}'S,S')Ni(L)](PF_6)_2$ (**37**) (Fig. 12). The Ni(II) centers in **37** reside in one square planar NiN_2S_2 (avg Ni–N: 1.99 Å; avg Ni–S: 2.15 Å) and one square planar NiP_2S_2 (avg Ni–P: 2.17 Å; avg Ni–S: 2.22 Å) coordination sphere. The two square planes are at 129° with a Ni–Ni distance of 2.99 Å. That the two P nuclei of **37** are equivalent is evident from the single resonance at 61.09 ppm in the $^{31}P\{^1H\}$ NMR spectrum of the complex in CD_2Cl_2 at room temperature. In CH_2Cl_2, **37** exhibits two reduction waves; a reversible electron process with $E_{1/2}$ = −0.47 V versus SCE (the Ni(I)/Ni(II) couple of the NiP_2S_2 moiety) and a second irreversible process at E_{red} = −1.22 V versus SCE. This second redox process has been attributed to either the Ni(0)/Ni(I) couple of the NiP_2S_2 moiety or the Ni(I)/Ni(II) couple of the NiN_2S_2 portion of the complex. Electrochemical reduction of **37** affords

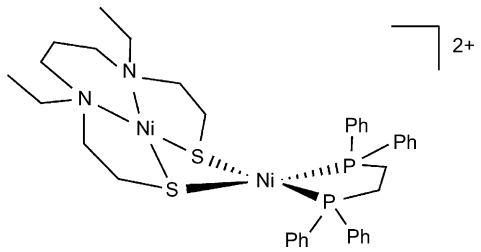

Fig. 12. Structure of $[(dppe)Ni^{II}(\mu\text{-}'S,S')Ni^{II}(L)]^{2+}$ (cation of **37**).

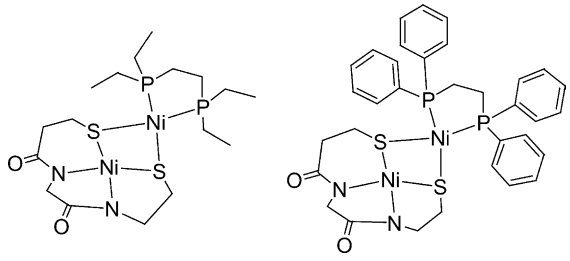

Fig. 13. Structures of $[\{Ni^{II}(L\text{-}655)\}Ni^{II}(depe)]$ (**38**) (left) and $[\{Ni^{II}(L\text{-}655)\}Ni^{II}(dppe)]$ (**39**) (right).

a reduced species that exhibits a nearly axial (g_1 = 2.158, g_2 = 2.050, g_3 = 2.040) and ^{31}P hyperfine-split EPR spectrum similar to those reported for other monomeric $[(dppe)NiS_2]$ species with Ni in the +1 oxidation state [70]. In addition, the EPR spectrum indicates that the two ^{31}P nuclei in reduced **37** are inequivalent most likely due to a change in coordination geometry at the metal center of the NiP_2S_2 moiety upon reduction. The two features of the Ni(II) center of the NiP_2S_2 unit of **37**, namely, the relatively positive reduction potential (due to the strongly π-accepting phosphine ligand) and change in coordination geometry (from square planar to tetrahedral) make it a close mimic of the Ni_p site in the A-cluster.

Holm and coworkers have also structurally characterized two binuclear Ni(II) models with phosphine ligands namely, [{Ni(L-655)}Ni(depe)] (**38**) and [{Ni(L-655)}Ni(dppe)] (**39**), that have been synthesized by a route similar to that of Schröder (Fig. 13) [71]. However, in these complexes, a more accurate Ni_d model with the exact same donor set and disposition of the A-cluster is employed (6-5-5 chelate ring pattern of the Cys-Gly-Cys protein sequence, Fig. 13). These red brown complexes exhibit a planar Ni-P_2S_2 bridged to an NiN_2S_2 unit with average Ni–Ni separation of 2.925(1) and 2.815(1) Å for **38** and **39**, respectively. To date, no other spectroscopic and/or reactivity properties of these complexes have been reported.

Recently, Mascharak and coworkers have reported the syntheses and structural characterization of a series of bi- and trinuclear Ni complexes as part of their modeling work [55,67]. Reaction of 2 equiv. of **15** with 1 equiv. of $[NiCl_4]^{2-}$ in MeCN affords the dark red trimeric complex $(Et_4N)_2[Ni\{Ni(NpPepS)\}_2]$ (**40**), which adopts a 'slant chair' structure with three coplanar Ni^{2+} centers (Fig. 14) [67]. The central Ni (designated Ni_C) in this species serves as a good structural model of the Ni_p site in ACS. When **40** is stirred in DMF, the initial slurry turns homogeneous within 15 min. The structure of the paramagnetic (S = 1) solid isolated from this bright red solution namely, $(Et_4N)_2[Ni(DMF)_2\{Ni(NpPepS)\}_2]$ (**41**) reveals two DMF molecules coordinated to Ni_C in *cis* fashion along with structural rearrangement of the two terminal $[Ni(NpPepS)]^{2-}$ units (Fig. 14). Comparison of the metric parameters of the octahedral Ni_C in **41** (Ni–S: 2.47 Å; Ni–Ni: 3.37 Å) with the square planar Ni_C in **40** (Ni–S: 2.23 Å; Ni–Ni: 3.24 Å) shows significant increases in the Ni–S and Ni–Ni bond distances

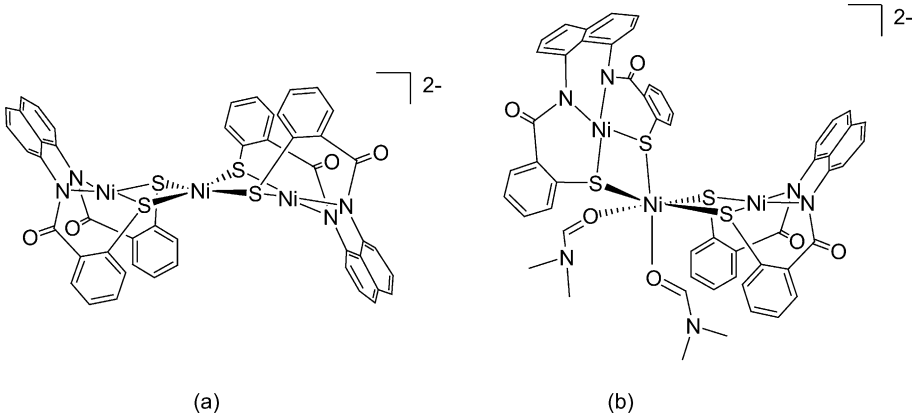

Fig. 14. Structures of: (a) $[Ni^{II}\{Ni^{II}(NpPepS)\}_2]^{2-}$ (anion of **40**); (b) $[Ni^{II}(DMF)_2\{Ni^{II}(NpPepS)\}_2]^{2-}$ (anion of **41**).

upon expansion of the coordination sphere. It is interesting to note that the Ni_C center in **40** expands its coordination sphere much like the Ni_p center in ACS and binds small molecules (DMF) in *cis* positions much like that proposed in one of the mechanisms for acetyl CoA synthesis [5]. Addition of reducing agents like $Na_2S_2O_4$ or $NaBH_4$ to **41** in DMF affords a species $\mathbf{41}_{red}$ with an axial EPR signal with $g = 2.33$ and 2.09 (100 K, DMF glass), consistent with a Ni(I) center in a distorted tetrahedral coordination sphere. Passage of CO through the solution of $\mathbf{41}_{red}$ in DMF gives rise to the CO-adduct $\mathbf{41}_{red}$**–CO**, that exhibits ν_{co} at 1960 cm^{-1}, consistent with a terminal Ni(I)–CO unit (Scheme 3). No reaction with CO is observed with either a solution of **41** in DMF or a solution of the monomeric complex **15** in DMF under similar reducing conditions. Furthermore, phen removes Ni_C from **41**, as in ACS, to afford **15** and $[Ni(phen)_3]^{2+}$. This reaction is rapid in DMF solution and can be conveniently monitored by electronic absorption spectroscopy. Addition of up

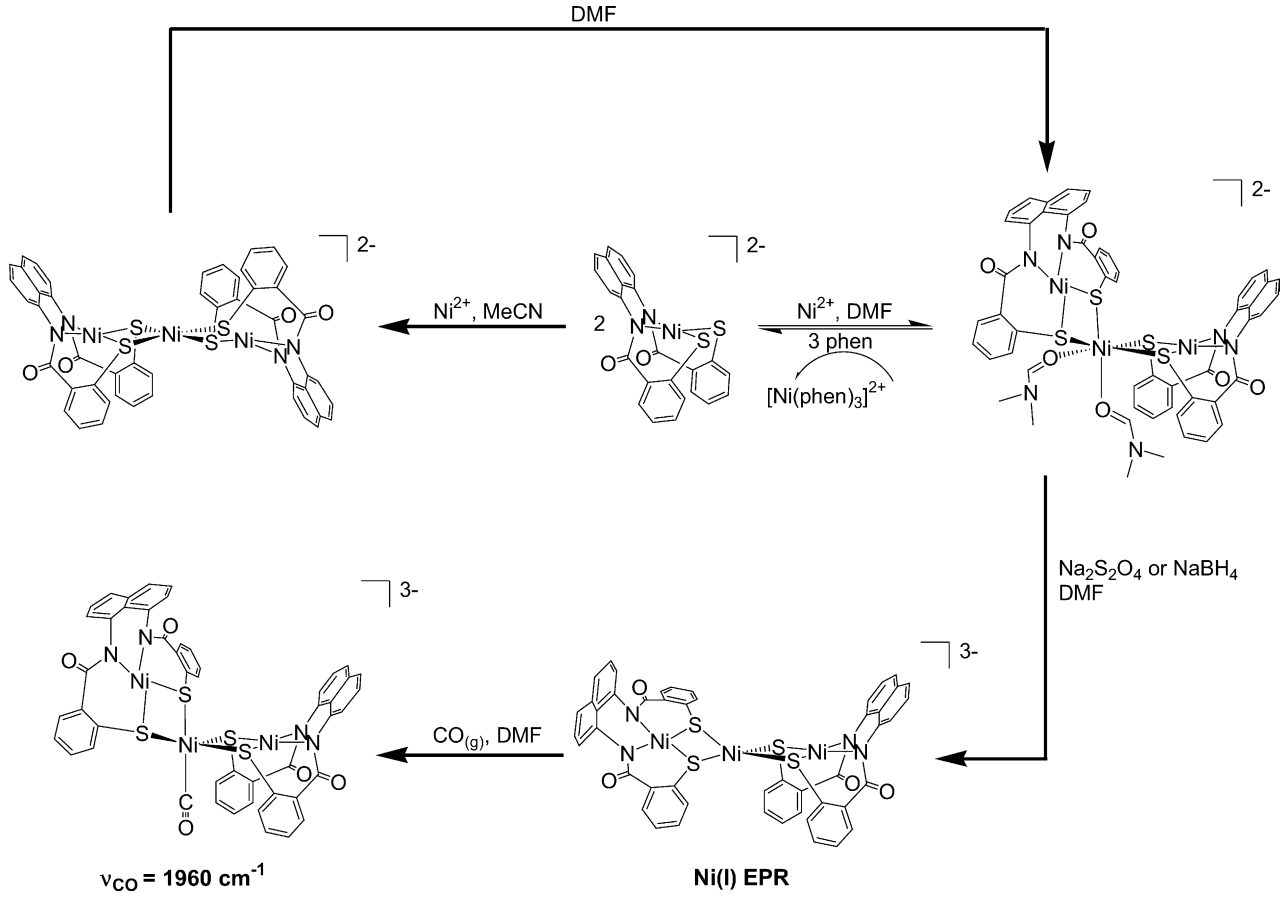

Scheme 3.

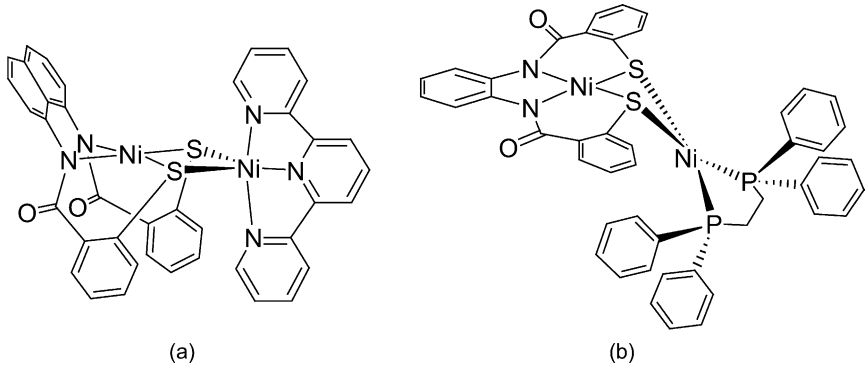

Fig. 15. Structures of: (a) [Ni^{II}(terpy)Ni^{II}(NpPepS)] (**42**); (b) [Ni^{II}(dppe)Ni^{II}(PhPepS)] (**43**).

to 100 equiv. phen to **15** or **41** results in no further change in the electronic absorption spectrum suggesting that Ni_d is not the source of 'labile Ni' responsible for the ACS activity. Complex **41** is the first example of a multinuclear model with carboxamide coordination to Ni(II) that mimics several properties of the A-cluster of ACS/CODH. The reactions of the trimeric species **40** and **41** are schematically shown in Scheme 3. Also, the chemical behavior of the Ni_C center of **41** (reduction and CO binding) lends further support in favor of Ni at the M_p site in catalytically active ACS.

Mascharak and coworkers have also synthesized two binuclear sulfur-bridged Ni–Ni models and studied their reactivity with reductants and CO [55]. Reaction of [Ni(terpy)Cl_2] (terpy = 2,2′:6′,2″-terpyridine) and **15** (1:1 ratio) in MeCN affords the neutral complex [Ni(terpy)Ni(NpPepS)] (**42**) as a red-brown powder in 75% yield (Fig. 15). An irreversible reduction wave is observed in the cyclic voltammogram of **42** in DMF with $E_{red} = -1.13$ V versus SCE. Reduction of **42** with $Na_2S_2O_4$ in DMF gives rise to $\mathbf{42}_{red}$ that exhibits an axial EPR spectrum with $g = 2.23$ and 2.13 (100 K). The EPR spectrum of $\mathbf{42}_{red}$ is very similar to that of other five-coordinate Ni(I) complexes in trigonal bipyramidal geometry [72]. Reaction of CO with $\mathbf{42}_{red}$ in DMF results in $\mathbf{42}_{red}$**–CO** adduct with terminal Ni(I)–CO band at 2044 cm^{-1}. Also, the EPR spectrum changes to a rhombic one ($g = 2.22$, 2.13, 2.02, DMF glass), typical of similar six-coordinate Ni(I) compounds with a terminally bound CO molecule [72,73]. Since **42** does not exhibit any affinity toward CO, it is evident that the Ni_p mimic in this model binds CO only in the reduced (+1) state.

The blue-green binuclear Ni–Ni model [Ni(dppe)Ni(PhPepS)] (**43**, Fig. 15) has been isolated from the reaction of [Ni(dppe)Cl_2] (dppe = 1,2-bis(diphenylphosphino)ethane) with **16** in MeCN [55]. In this Ni–Ni model, the two Ni(II) centers are bridged through the two thiolato-S donors of the $PhPepS^{4-}$ ligand frame and both exist in square planar geometry. The dihedral angle between the two square planes is 111.4° and the Ni–Ni separation is 2.8255(4) Å. The metric parameters of the bridged Ni_d synthon **16** are very similar to that noted in **43**. This suggests that sulfur metalation does not change any structural feature of this Ni_d mimic. Complex **43** can be easily reduced with $Na_2S_2O_4$ or $NaBH_4$ and $\mathbf{43}_{red}$ exhibits a Ni(I) EPR spectrum ($g = 2.25$, 2.12, 2.07) similar to other Ni(I)P_2S_2 complexes [70]. Although **43** displays no reactivity towards CO, passage of CO through a DMF solution of $\mathbf{43}_{red}$ generates the CO-adduct $\mathbf{43}_{red}$**–CO** that displays a strong ν_{co} band at 1997 cm^{-1} consistent with a terminal Ni(I)–CO unit. One must note that this ν_{co} value is very close to the enzyme value of 1996 cm^{-1} [10]. Additionally, treatment of **43** with excess phen (~25 equiv.) in CH_2Cl_2 removes the Ni_p mimic resulting in the formation of monomer **16** and $[Ni(phen)_3]^{2+}$ over a time period of ~35 min. This reaction confirms that the thiolato-S bridges between the Ni_d and the Ni_p centers in models like **43** are vulnerable to phen treatment. Since phen does not remove Ni from the Ni_d synthons **15** and **16**, it is again apparent that the 'labile Ni' in the enzyme arises from the Ni_p site. It is important to note that **42** and **43** are some of the first structurally and spectroscopically characterized examples of sulfur-bridged binuclear Ni compounds with terminal Ni-dicarboxamido-dithiolato units that bind CO to a Ni(I) center as proposed in case of the A-cluster of ACS/CODH.

4. Conclusions

The results of the modeling work performed by various groups so far have revealed valuable information regarding the novel A-cluster involved in acetyl CoA synthesis by ACS/CODH. For example, it is quite evident that coordination of both carboxamido nitrogen and thiolato sulfur stabilizes the Ni(II) state to a great extent and hence the Ni_d site is not expected to participate in any chemistry in the +1 oxidation state. Binding of potential substrate(s) at such site is also unlikely. Quite in contrast, the Ni_p site appears to be reducible. The Ni(I) centers in the reduced models can expand their coordination spheres and bind CO in terminal fashion with ν_{co} values similar to that in ACS/CODH. Also, it is now quite clear that it is Ni and not Cu that is present at the M_p site in catalytically active A-cluster. The model studies have provided strong hint toward the source of 'labile Ni' in ACS/CODH. Although the Ni_p mimics (coordinated

by metallosulfur donors) in models such as **27** and **41** are removable with phen, Ni cannot be taken out from the NiN_2S_2 units (Ni_d mimics) in all cases. This strongly supports that the hypothesis that Ni at M_p site is the source of 'labile Ni' in the enzyme. It is therefore reasonable to expect that the syntheses and studies on more robust and functional model complexes will keep on adding insight into the catalytic mechanism of the unique metallocluster site of ACS/CODH. In a recent issue of the Journal of Biological Inorganic Chemistry, several commentaries on the ACS/CODH enzyme and one on the synthetic models lend support to this expectation [37,74–78].

Since modeling studies so far have not incorporated the Fe_4S_4 cubane in the models, it is not clear what kind of changes in the chemical and redox behaviors the models will undergo upon inclusion of the iron-sulfur cluster. Although all the proposed mechanisms involve electron transfer to and from the Fe_4S_4 cubane, recent studies have indicated that such electron flow is too slow compared to the rate of the methyl transfer [6], a fact that raises questions regarding direct participation of the Fe_4S_4 cubane in the catalytic cycle. On the other hand, spectroscopic evidences suggest coupling of the Fe_4S_4 cubane with the Ni_p–Ni_d moiety. In addition, results of theoretical studies indicate that such coupling could support Ni(0) at the Ni_p site [23,37,79]. Clearly, the next generation models of the ACS A-cluster have to incorporate the Fe_4S_4 cubane in order to address this issue [80]. An attempt in this direction has recently been initiated by Holm and coworkers [81]. However, only the thiolato-bridged $[Fe_4S_4]$–NiL type of structures has been isolated. It is reasonable to anticipate that the $[Fe_4S_4]$–Ni_p–Ni_d type of models will remain as synthetic challenge for some time due to complications associated with the assembly of designed heterometallic clusters via thiolato bridges.

References

[1] S.W. Ragsdale, M. Kumar, Chem. Rev. 96 (1996) 2515.
[2] P.A. Lindahl, Biochemistry 41 (2002) 2097.
[3] H.G. Wood, L.G. Ljungdahl, Variation in Autotrophic Life, Academic Press, New York, 1991.
[4] T.I. Doukov, T.M. Iverson, J. Seravalli, S.W. Ragsdale, C.L. Drennan, Science 298 (2002) 567.
[5] C. Darnault, A. Volbeda, E.J. Kim, P. Legrand, Z. Vernede, P.A. Lindahl, J.C. Fontecilla-Camps, Nat. Struct. Biol. 10 (2003) 271.
[6] X. Tan, C. Sewell, Q. Yang, P.A. Lindahl, J. Am. Chem. Soc. 125 (2003) 318.
[7] S.W. Ragsdale, H.G. Wood, W.E. Antholine, Proc. Natl. Acad. Sci. U.S.A. 82 (1985) 6811.
[8] C.M. Gorst, S.W. Ragsdale, J. Biol. Chem. 266 (1991) 20687.
[9] M. Kumar, S.W. Ragsdale, J. Am. Chem. Soc. 114 (1992) 8713.
[10] J. Chen, S. Huang, J. Seravalli, H. Gutzman Jr., D.J. Swartz, S.W. Ragsdale, K.A. Bagley, Biochemistry 42 (2003) 14822.
[11] W. Shin, P.A. Lindahl, J. Am. Chem. Soc. 114 (1992) 9718.
[12] M.R. Bramlett, X. Tan, P.A. Lindahl, J. Am. Chem. Soc. 125 (2003) 9316.
[13] D.P. Barondeau, P.A. Lindahl, J. Am. Chem. Soc. 119 (1997) 3959.
[14] X.S. Tan, C. Sewell, P.A. Lindahl, J. Am. Chem. Soc. 124 (2002) 6277.
[15] J.Q. Xia, Z.G. Hu, C.V. Popescu, P.A. Lindahl, E. Munck, J. Am. Chem. Soc. 119 (1997) 8301.
[16] W.K. Russell, C.M.V. Stalhandske, J. Xia, R.A. Scott, P.A. Lindahl, J. Am. Chem. Soc. 120 (1998) 7502.
[17] E.L. Maynard, C. Sewell, P.A. Lindahl, J. Am. Chem. Soc. 123 (2001) 4697.
[18] H. Dobbek, V. Svetlitchnyi, L. Gremer, R. Huber, O. Meyer, Science 293 (2001) 1281.
[19] C.L. Drennan, J. Heo, M.D. Sintchak, E. Schreiter, P.W. Ludden, Proc. Natl. Acad. Sci. U.S.A. 98 (2001) 11973.
[20] J. Seravalli, W. Gu, A. Tam, E. Strauss, T.P. Begley, S.P. Cramer, S.W. Ragsdale, Proc. Natl. Acad. Sci. U.S.A. 100 (2003) 3689.
[21] J. Seravalli, Y. Xiao, W. Gu, S.P. Cramer, W.E. Antholine, V. Krymov, G.J. Gerfen, S.W. Ragsdale, Biochemistry 43 (2004) 3944.
[22] C.E. Webster, M.Y. Darensbourg, P.A. Lindahl, M.B. Hall, J. Am. Chem. Soc. 126 (2004) 3410.
[23] R.P. Schenker, T.C. Brunold, J. Am. Chem. Soc. 125 (2003) 13962.
[24] S. Gencic, D.A. Grahame, J. Biol. Chem. 278 (2003) 6101.
[25] T. Funk, W. Gu, S. Friedrich, H. Wang, S. Gencic, D.A. Grahame, S.P. Cramer, J. Am. Chem. Soc. 126 (2004) 88.
[26] V. Svetlitchnyi, H. Dobbek, W. Meyer-Klaucke, T. Meins, B. Thiele, P. Römer, R. Huber, O. Meyer, Proc. Natl. Acad. Sci. U.S.A. 101 (2004) 446.
[27] J.W. Peters, M.H. Stowell, M. Soltis, M.G. Finnegan, M.K. Johnson, D.C. Rees, Biochemistry 36 (1997) 1181.
[28] S. Nagashima, M. Nakasako, N. Dohmae, M. Tsujimura, K. Takio, M. Odaka, M. Yohda, N. Kamiya, I. Endo, Nat. Struct. Biol. 5 (1998) 347.
[29] D.P. Barondeau, C.J. Kassmann, C.K. Bruns, J.A. Tainer, E.D. Getzoff, Biochemistry 43 (2004) 8038.
[30] E. Murakami, S.W. Ragsdale, J. Biol. Chem. 275 (2000) 4699.
[31] J. Seravalli, M. Kumar, S.W. Ragsdale, Biochemistry 41 (2002) 1807.
[32] H.-F. Klein, H.H. Karsch, Angew. Chem., Int. Ed. Engl. 12 (1973) 402.
[33] P. Stavropoulos, M.C. Muetterties, M. Carrie, R.H. Holm, J. Am. Chem. Soc. 113 (1991) 8485.
[34] Y.-M. Hsiao, S.S. Chojnacki, P. Hinton, J.H. Reibenspies, M.Y. Darensbourg, Organometallics 12 (1993) 870.
[35] G.C. Tucci, R.H. Holm, J. Am. Chem. Soc. 117 (1995) 6489.
[36] C.S. Shultz, J.M. DeSimone, M. Brookhart, J. Am. Chem. Soc. 123 (2001) 9172.
[37] P.A. Lindahl, J. Biol. Inorg. Chem. 9 (2004) 516.
[38] J.A. Ibers, R.H. Holm, Science 209 (1980) 223.
[39] I.G. Dance, Polyhedron 5 (1986) 1037.
[40] C.A. Grapperhaus, M.Y. Darensbourg, Acc. Chem. Res. 31 (1998) 451.
[41] T. Herskovitz, B.V. Depamphilis, W.O. Gillum, R.H. Holm, Inorg. Chem. 14 (1975) 1426.
[42] K.J. Ellis, A.G. Lappin, A. McAuley, J. Chem. Soc., Dalton Trans. (1975) 1930.
[43] L. Sacconi, P. Dapporto, P. Stoppioni, P. Innocenti, C. Benelli, Inorg. Chem. 16 (1977) 1669.
[44] A. Bakac, J.H. Espenson, J. Am. Chem. Soc. 108 (1986) 713.
[45] P. Stoppioni, P. Dapporto, L. Sacconi, Inorg. Chem. 17 (1978) 718.
[46] G. Wilke, G. Herrmann, Angew. Chem., Int. Ed. Engl. 5 (1966) 581.
[47] P.J. Schebler, C.G. Riordan, I.A. Guzei, A.L. Rheingold, Inorg. Chem. 37 (1998) 4754.
[48] P.J. Schebler, B.S. Mandimutsira, C.G. Riordan, L.M. Liable-Sands, C.D. Incarvito, A.L. Rheingold, J. Am. Chem. Soc. 123 (2001) 331.
[49] J.L. Craft, B.S. Mandimutsira, K. Fujita, C.G. Riordan, T.C. Brunold, Inorg. Chem. 42 (2003) 859.
[50] H.-J. Krüger, R.H. Holm, Inorg. Chem. 26 (1987) 3645.
[51] H.-J. Krüger, G. Peng, R.H. Holm, Inorg. Chem. 30 (1991) 734.
[52] J.C. Dutton, G.D. Fallon, K.S. Murray, Chem. Lett. (1990) 983.
[53] J. Hanss, H.-J. Krüger, Angew. Chem. Int. Ed. 37 (1998) 360.
[54] T.C. Harrop, M.M. Olmstead, P.K. Mascharak, Inorg. Chim. Acta 338 (2002) 195.

[55] T.C. Harrop, M.M. Olmstead, P.K. Mascharak, J. Am. Chem. Soc. 126 (2004) 14714.
[56] Ø. Hatlevik, M.C. Blanksma, V. Mathrubootham, A.M. Arif, E.L. Hegg, J. Biol. Inorg. Chem. 9 (2004) 238.
[57] R.C. Linck, C.W. Spahn, T.R. Rauchfuss, S.R. Wilson, J. Am. Chem. Soc. 125 (2003) 8700.
[58] P.J. Farmer, J.H. Reibenspies, P.A. Lindahl, M.Y. Darensbourg, J. Am. Chem. Soc. 115 (1993) 4665.
[59] G. Musie, P.J. Farmer, T. Tuntulani, J.H. Reibenspies, M.Y. Darensbourg, Inorg. Chem. 35 (1996) 2176.
[60] Even neutral Ni(II) complexes bearing diamine-dithiolato ligands like [(BME-DACO)Ni] show no observable reduction in the same potential range;
D.K. Mills, J.H. Reibenspies, M.Y. Darensbourg, Inorg. Chem. 29 (1990) 4364.
[61] R. Krishnan, J.K. Voo, C.G. Riordan, L. Zahkarov, A.L. Rheingold, J. Am. Chem. Soc. 125 (2003) 4422.
[62] C. Ohrenberg, C.G. Riordan, L.M. Liable-Sands, A.L. Rheingold, Inorg. Chem. 40 (2001) 4276.
[63] P.J. Farmer, T. Solouki, D.K. Mills, T. Soma, D.H. Russell, J.H. Reibenspies, M.Y. Darensbourg, J. Am. Chem. Soc. 114 (1992) 4601.
[64] M.A. Turner, W.L. Driessen, J. Reedjik, Inorg. Chem. 29 (1990) 3331.
[65] T. Tuntulani, J.H. Reibenspies, P.J. Farmer, M.Y. Darensbourg, Inorg. Chem. 31 (1992) 3497.
[66] M.L. Golden, M.V. Rampersad, J.H. Reibenspies, M.Y. Darensbourg, Chem. Commun. (2003) 1824.
[67] T.C. Harrop, M.M. Olmstead, P.K. Mascharak, Chem. Commun. (2004) 1744.
[68] R. Krishnan, C.G. Riordan, J. Am. Chem. Soc. 126 (2004) 4484.
[69] Q. Wang, A.J. Blake, E.S. Davies, E.J.L. McInnes, C. Wilson, M. Schröder, Chem. Commun. (2003) 3012.
[70] G.A. Bowmaker, P.D.W. Boyd, G.K. Campbell, Inorg. Chem. 21 (1982) 2403.
[71] P.V. Rao, S. Bhaduri, J. Jiang, R.H. Holm, Inorg. Chem. 43 (2004) 5833.
[72] N. Baidya, M.M. Olmstead, J.P. Whitehead, C. Bagyinka, M.J. Maroney, P.K. Mascharak, Inorg. Chem. 31 (1992) 3612.
[73] C.A. Marganian, H. Vazir, N. Baidya, M.M. Olmstead, P.K. Mascharak, J. Am. Chem. Soc. 117 (1995) 1584.
[74] C.L. Drennan, T.I. Doukov, S.W. Ragsdale, J. Biol. Inorg. Chem. 9 (2004) 511.
[75] A. Volbeda, J.C. Fontecilla-Camps, J. Biol. Inorg. Chem. 9 (2004) 525.
[76] T.C. Brunold, J. Biol. Inorg. Chem. 9 (2004) 533.
[78] C.G. Riordan, J. Biol. Inorg. Chem. 9 (2004) 542.
[79] P. Amara, A. Volbeda, J.C. Fontecilla-Camps, M.J. Field, J. Am. Chem. Soc. 127 (2005) 2776.
[80] E.L. Hegg, Acc. Chem. Res. 37 (2004) 775.
[81] P.V. Rao, S. Bhaduri, J. Jiang, D. Hong, R.H. Holm, J. Am. Chem. Soc. 127 (2005) 1933.